Draft version October 4, 2024
Typeset using LaTeX **twocolumn** style in AASTeX631

Time Variation of the Solar Tachocline

Sarbani Basu,[1] Wesley Antônio Machado Andrade de Aguiar,[2] and Sylvain G. Korzennik[3]

[1] *Department of Astronomy, Yale University, PO Box 208101, New Haven, CT 06520-8101, USA*
[2] *Department of Computer Science, Yale University, PO Box 208285, New Haven, CT 06520-8285, USA*
[3] *Center for Astrophysics | Harvard & Smithsonian, Cambridge, MA 02138, USA*

Submitted to ApJ

ABSTRACT

We have used solar oscillation frequencies and frequency splittings obtained over solar cycles 23, 24 and the rising phase of solar cycle 25 to investigate whether the tachocline properties (jump i.e., the change in the rotation rate across the tachocline, width and position) show any time variation. We confirm that the change in rotation rate across the tachocline changes substantially, however, the change does not show a simple correlation with solar cycle unlike, for instance, changes in mode frequencies. The change during the ascending phase of solar cycle 25 is almost a mirror image of the change during the descending part of solar cycle 24, tempting us to speculate that the tachocline has a much longer period than either the sunspot or the magnetic cycle. We also find that the position of the tachocline, defined as the mid-point of the change in rotation rate, showed significant changes during solar cycle 24. The width of the tachocline, on the other hand, has showed significant changes during solar cycle 23, but not later. The change in the tachocline becomes more visible if we look at the upper and lower extents of the tachocline, defined as (position ± width). We find that for epochs around solar maxima and minima, the extent decreases before increasing again — a few more years of data should clarify this trend. Our results reinforce the need to continue helioseismic monitoring of the Sun to understand solar activity and its evolution.

Keywords: The Sun (1693) — solar cycle (1487) — solar oscillations (1515) — helioseismology (709) — solar rotation (1524)

1. INTRODUCTION

Helioseismic analyses have shown that the convection zone (henceforth CZ) of the Sun rotates differentially, while the radiative interior rotates like a solid body (Schou et al. 1998, etc.). Connecting the two zones is a thin shear layer, known as the tachocline.

Neither the origin of the tachocline nor the role it plays is well understood. This layer is often cited as a key region in the process of magnetic field generation in the Sun and other solar-like stars, as it is a region of strong shear and therefore capable of converting weak poloidal fields into strong toroidal fields. Some dynamo models of the Sun (Dikpati & Charbonneau 1999; Chatterjee et al. 2004; Guerrero & de Gouveia Dal Pino 2008) assume that the large-scale toroidal magnetic field generated at the tachocline can, when strong enough, move up to the surface and manifest as sunspots. In fact, in 3D MHD simulations of the solar dynamo that include the tachocline, most of the magnetic field develops at the base of the convection zone (Guerrero et al. 2016). It has also been argued that the tachocline plays a key role in establishing the period of the solar cycle, the origin of torsional oscillations, and the scaling law of stellar magnetic fields as a function of the Rossby number (Guerrero et al. 2017).

If indeed the tachocline is responsible for the changing magnetic fields in the Sun, one could expect that the tachocline varies on solar-cycle timescales. It has been shown by Basu & Antia (2019) that the change in the rotation rate between the solar CZ and the radiative zone (the "jump") is a function of time; however, the temporal dependence is not a simple correlation with magnetic activity. The jump followed different trends during solar cycle 23 than solar cycle 24 and, furthermore, had different values at the same level of solar activity. Basu & Antia (2019) could not, however,

detect any changes in the position of the tachocline or the width of the tachocline; the uncertainty of their result was too large due to the lack of precision of the data sets they used. The data sets used in that study were splitting coefficients obtained with 108-day long time series from the Global Oscillation Network Group (GONG: Hill et al. 1996) along with those obtained using 72-day long time series from the Michelson Doppler Imager (MDI: Scherrer et al. 1995) on board the Solar and Heliospheric Observatory (SOHO) and the Helioseismic and Magnetic Imager (HMI: Scherrer et al. 2012) on board the Solar Dynamics Observatory (SDO). An earlier attempt by Antia & Basu (2011) using data from the same sources was also unsuccessful in detecting any clear changes in the thickness of the tachocline, although they did observe changes in the jump and possible changes in the position.

Changes in the thickness of the tachocline could help distinguish between dynamo models of the Sun. For instance, Dikpati & Gilman (2001) claim that if toroidal fields are concentrated in relatively narrow bands that migrate towards the equator as the sunspot cycle advances, then they should be accompanied by a "thickness front" advancing at the same rate. The position of the tachocline may also change — among the different scenarios proposed to explain the relatively weak solar activity between 2005 and 2010, one hypothesis attributes it to small "pulsations" in the position of the tachocline (de Jager et al. 2016).

The time series used in earlier investigations into tachocline properties were too short to obtain frequency splitting coefficients precise enough to reliably determine changes in the position and thickness of the tachocline. The situation has since changed and splitting coefficients derived from longer time series are now available, and in addition we have data spanning more than two solar cycles. In this paper, we use frequency splittings obtained with different lengths of helioseismic time series to determine temporal variations in the position and thickness of the tachocline.

The rest of this paper is organized as follows. We describe the data used in § 2, the tachocline model, and how we determined the tachocline properties in § 3. Our results are described in § 4, and we discuss the results in § 5.

2. DATA USED

For this work, we use solar oscillation frequencies derived from observations obtained with the ground-based GONG network and the space-borne MDI and HMI instruments on board the Solar & Heliospheric Observatory (SOHO) and the Solar Dynamics Observatory (SDO) respectively. MDI observations started in 1995 and ended in 2010, hence they cover solar cycle 23, while HMI observations started in 2010 and are continuing, hence HMI observations cover cycles 24 and 25. There is a one-year overlap between MDI and HMI observations.

We use rotational frequency splittings obtained by an independent data reduction pipeline (Korzennik 2004, 2008a,b; Korzennik & Eff-Darwich 2013; Korzennik 2017, 2018, 2023), which we refer to as the "SGK" pipeline. The SGK pipeline derives mode parameters from time series that are multiples of 72 days, therefore we use mode frequencies and splittings obtained for time series lengths of 32×, 16×, 10×, 8× and 5 × 72 days, or approximately 6, 3, 2, 1.5 and 1 year, respectively. The choice of using multiples of 72-days was dictated by the standard time series length adopted initially by the MDI team, and later adopted by the HMI team. At the time, a time series of 72 days was considered to be long enough to produce a power spectrum with high signal-to-noise ratio, but short enough to provide "good" temporal resolution of the inferred frequencies and frequency splittings. The MDI and HMI teams later started analyzing 360-day (i.e., 5 × 72-day) long time series too. We also use splittings from the respective teams pipelines (henceforth referred to simply as "pipeline data") to compare to results obtained with the splittings inferred with the SGK pipeline.

The SGK pipeline predominantly derives mode parameters by fitting asymmetric profiles to peaks in the power spectra, though some data sets have also been fitted using symmetric profiles. The MDI and HMI projects' pipeline, on the other hand, generally fits symmetric profiles, though some 360-day long sets have been fitted with asymmetric profiles.

The starting dates of all SGK sets are equally spaced in time, aligned with the first 72-day long MDI set (i.e., 1995.05.01). The MDI and HMI 5 × 72-day long sets from the projects' pipeline, however, do not always have equal spacings, and some of the start dates of the project's and SGK sets differ. The start times of all sets that we analyzed are listed in the tables in Appendix B.

The data sets are available in the usual form, where the mode frequencies and their splittings are expressed as follows:

$$\nu_{nlm} = \nu_{nl} + \sum_{j=1}^{j_{\max}} a_j(n,l)\, \mathcal{P}_j^{(l)}(m), \qquad (1)$$

where ν_{nl}, or the central frequency of a mode of degree l and radial order n, is determined by the spherically symmetric part of solar structure, a_j are splitting coefficients and $\mathcal{P}_j$ are re-scaled Clebsch-Gordon coef-

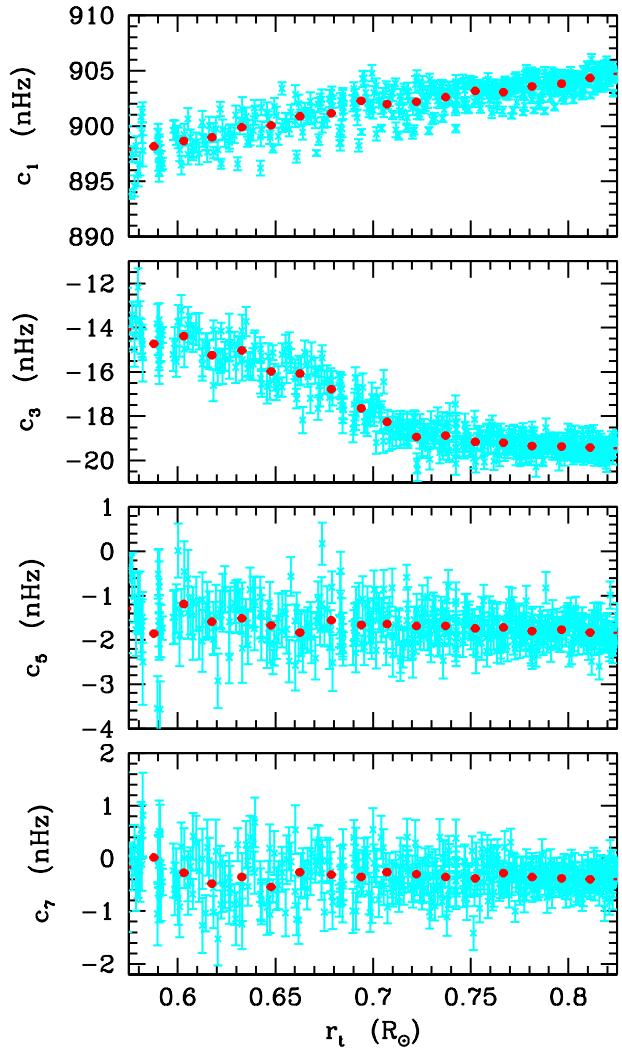

Figure 1. Odd-order splitting coefficients, c_1–c_5, derived from a 16 × 72-day long time series plotted as a function of the lower turning points of the modes. The cyan points are the individual values, while the red points show values averaged over r_t bins of width $0.015R_\odot$. The error bars on the red points are not visible because they are similar to the size of the symbols.

ficients (see Schou et al. 2002). In this decomposition, the odd-order a_j are caused by the solar rotation, while the even-order coefficients contain the signature of asphericity and magnetic fields. In order to compare with earlier work, we convert the a coefficients to c coefficients as defined by Ritzwoller & Lavely (1991).

The first four odd-order splitting coefficients for a 16 × 72-day long GONG time series plotted as a function of the lower-turning point[1] are shown in Fig. 1. That figure shows that the clearest signature of the tachocline is in the c_3 splittings, and is essentially the same as that shown in Fig. 10 of Basu (1997). There appears to be a small signature in c_1, while the other splitting coefficients are too noisy to show such a signal. Consequently, we only use the c_3 coefficient in the work presented here. Furthermore, we only use modes with frequencies between 1.5 mHz and 3.5 mHz that have lower turning points between $0.55R_\odot$ and $0.85R_\odot$ for the range of degrees that is covered by the data set. This subset of mode-splitting coefficients give good coverage of the tachocline, while keeping the uncertainties low; this also removes the need to account for the near-surface shear layer in the tachocline model.

3. TACHOCLINE MODEL AND ANALYSIS TECHNIQUE

We perform a forward analysis to determine tachocline properties. Following Ritzwoller & Lavely (1991), we express the solar rotation velocity, (see also Antia et al. 1998), as

$$v_{\rm rot}(r,\vartheta) = \Omega(r,\vartheta) r\sin\vartheta = -\sum_{s=0}^{\infty} w_{2s+1}(r)\frac{\partial}{\partial\vartheta}Y^0_{2s+1}, \quad (2)$$

where r is the radius, ϑ the co-latitude, $Y_l^m(\vartheta)$ are spherical harmonics and $w_s(r)$ are functions that are related to the splitting coefficients as follows:

$$c_s^{(n,l)} = \int_0^R w_s(r) K_s^{(n,l)} r^2 {\rm d}r, \quad (3)$$

where the kernels, $K_s^{(n,l)}$, are known functions of the displacement eigenfunctions of the modes (see Eq. 5 of Antia et al. 1998).

Eq. 2 essentially separates the radial and angular dependence of the rotation rate, and Eq. 3 shows how c_3 can can be calculated given a one dimensional rotation rate $\Omega(r)$, which in our case, is the model of the tachocline. At any colatitude ϑ, the rotation rate $\Omega(r,\vartheta)$ is simply

$$\Omega(r,\vartheta) = -\Omega(r)\frac{\partial}{\partial\vartheta}Y_3^0 = \Omega(r)\frac{3}{4}\sqrt{\frac{7}{\pi}}(1-5\cos^2\vartheta), \quad (4)$$

implying that there is no contribution from c_3 at a latitude of approximately 26.56°. Following Basu (1997),

[1] The lower turning point, r_t, is the deepest point that an acoustic mode propagates to. It can be evaluated through the relation $c_s^2/r_t^2 = \omega^2/L$, where c_s is the speed of sound, $\omega \equiv 2\pi\nu$, and $L = l(l+1)$.

we model the tachocline as a sigmoid and parametrize the rotation rate around the tachocline as

$$\Omega(r) = \frac{\delta\Omega}{1+\exp[-(r_d - r)/w_d]}, \quad (5)$$

where $\delta\Omega$ is the jump in the rotation rate between the convection zone and the interior, r_d is the position of the tachocline, defined as the mid-point of the transition (or discontinuity), and w_d is the width of the transition layer. With this parametrization, the rotation rate changes from 0.269 to 0.731 (i.e., from $1/(1+e)$ to $1-1/(1+e)$) of $\delta\Omega$ between radii of $r = e_d - w_d$ and $r = r_d + w_d$. The tachocline is located approximately at the base of the convection zone, i.e., r_d is about $0.71R_\odot$. Note that Antia et al. (1998), Antia & Basu (2011), and Basu & Antia (2019) used essentially the same model of the tachocline, but had co-latitude dependent terms since they did a full 2D fit. Also note that in this parametrization of the tachocline, the definition of the width is different from that used by Kosovichev (1996) and Charbonneau et al. (1999), where the tachocline was parametrized by an error-function, erf(r), namely $\Omega(r) = \delta\Omega(1+\mathrm{erf}(2(r-r_d)/w_d)/2$, where the width corresponds to the region where the rotation rate changes from 0.08 to 0.92 of the jump, $\delta\Omega$. For small widths, w_d, one can show that $w_d^{\mathrm{erf}} \approx 5\, w_d^{\mathrm{sigmoid}}$.

We used two minimization techniques to estimate the three parameters of the tachocline, namely $\delta\Omega$, r_d and w_d. One is based on a search within a pre-computed grid of models, while the another uses a simulated annealing (SA) optimization. These two methods are described in Appendix A. The grid-based method is very fast, while the SA method, even with only three parameters, is slow. However, as shown in Appendix A, the grid-based method does not recover the width of the tachocline very well, and since determining possible changes in the width of the tachocline is a major goal of this work, we only report results obtained with the SA method.

4. RESULTS

Since we are interested in examining the temporal variation of the tachocline, we examine results obtained with data sets corresponding to the shortest time series that we are considering, i.e., the 5×72-day long ones, before examining the longer sets.

4.1. *Results from* 5×72*-day sets*

The 360-day-long data sets are useful because they have been processed both with the MDI and HMI project pipelines, as well as the SGK pipeline. Furthermore, the mode parameters were obtained using both symmetric and asymmetric profiles. The resulting tachocline parameters are presented in Fig. 2 and tabulated in Tables 4 and 5 in Appendix B.

One can see from Fig. 2 that $\delta\Omega$, the jump across the tachocline, is the most well-determined property, and that the jump shows a very clear temporal variation, although the changes during cycle 23 were quite different from those during cycle 24. This is consistent with what was found by Basu & Antia (2019). We also find a systematic difference between the jump, obtained with the project pipeline data sets and those obtain with the SGK pipeline. Basu & Antia (2019) had seen a similar systematic difference between results from the GONG, MDI and HMI pipelines' data sets. Since we do not see any such difference between GONG, MDI and HMI observations processed with the SGK pipeline, we are led to believe that the root of this difference lies in the choices made in the projects' pipelines. Furthermore, one can also see that there is a systematic difference between the MDI and HMI pipeline results during the time when both projects were observing. While such systematic differences add to the uncertainty of $\delta\Omega$, we can see that it does not affect inferences about the temporal variation. We also see that results obtained when using splitting coefficients obtained using symmetric and asymmetric mode profiles are consistent with each other.

We also have a few data sets corresponding to the rising part of cycle 25, and we see that the change in the jump is again trending differently from the previous solar cycles. Indeed, the absolute value of the jump is decreasing, and has almost overcome the increase seen during the falling part of cycle 24. It will be interesting to see if by the end of cycle 25 the value of this jump will be back to the value it had at the end of cycle 23. If so, it would indicate the presence of a much longer activity cycle at the tachocline. Since shorter time series data allow us to add to the cycle 25 timeline, we show the jump results obtained with 72-day long time series in Fig. 3; although these results are noisier, the upward trend is clearly visible. From that same figure, one is tempted to infer that results obtained with GONG observations acquired during the last year of cycle 22 show a fall in $\delta\Omega$, which then becomes a rise in the ascending phase of cycle 23. These values are presented in Tables 1, 2 and 3 in Appendix B.

Returning to the 5×72-day long results, we find that the derived estimates of the tachocline mid-point are quite noisy, making it difficult to state whether the temporal variations are statistically significant over the entire timeline. The results derived from symmetric mode-profile fits appear to be more scattered than those derived from asymmetric mode-profile fits. Whether the

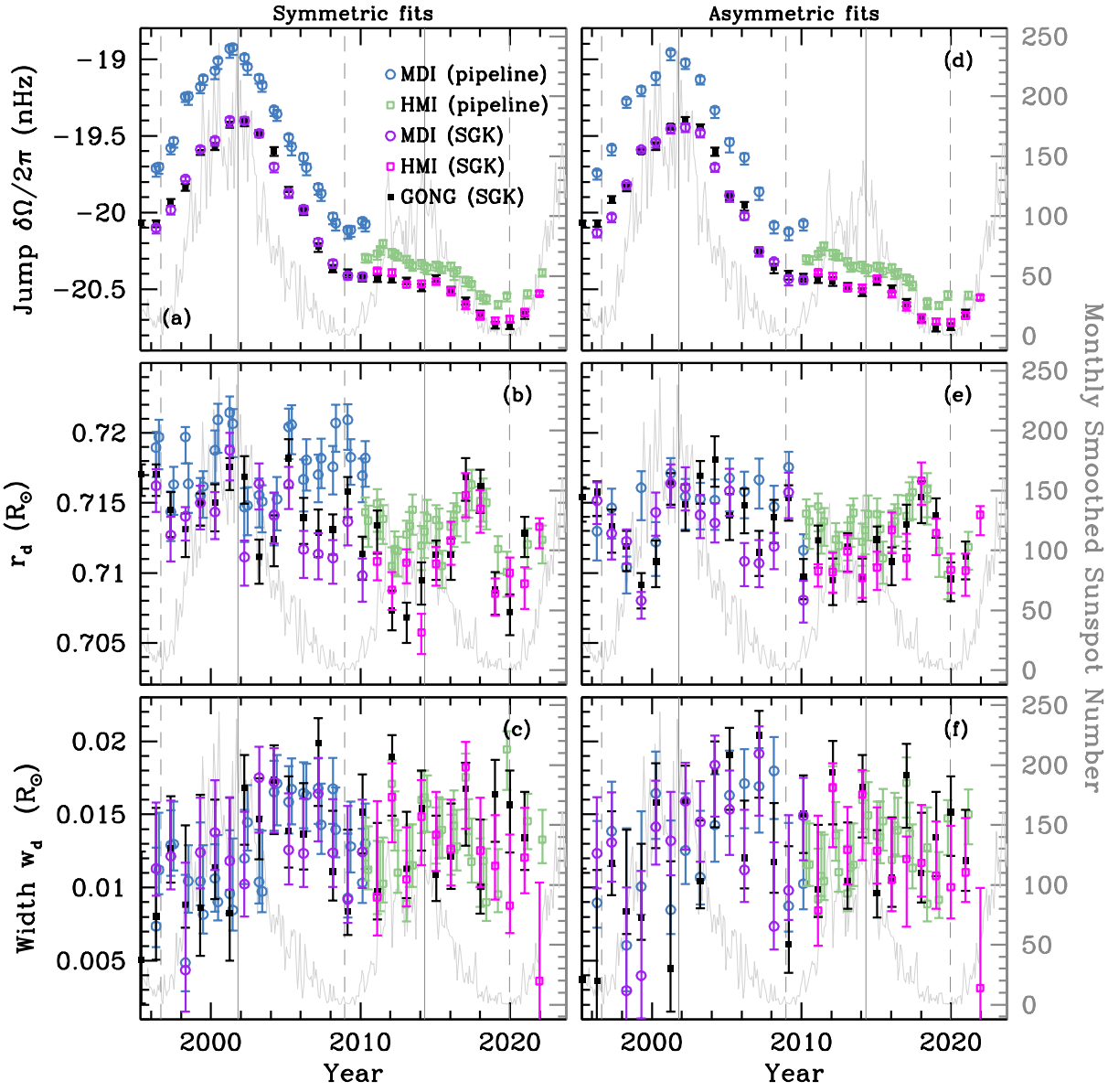

Figure 2. Tachocline properties estimated using data sets obtained with 5×72-day long time series plotted as a function of time, using the time at the mid-point of the observational window. The panels on the left were obtained for data with symmetric fits to the mode profile, while those on the right with asymmetric profiles. The different colors and symbols correspond to data sets corresponding to GONG, MDI or HMI observations using either the MDI or HMI projects' pipelines or the SGK pipeline as shown in the legend. The gray curve shows the monthly smoothed sunspot numbers from the Royal Observatory of Belgium, Brussels, whose scale can be read on the right-hand axes. The vertical solid lines mark the times of solar maximum, while the vertical dashed lines mark the times of solar minimum determined from smoothed values of activity proxies.

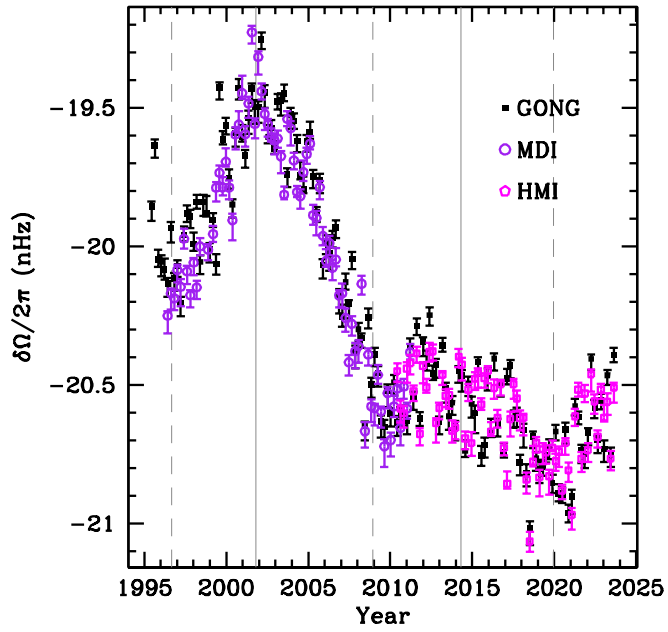

Figure 3. The jump across the tachocline derived from the 72-day long time series data sets using GONG, MDI or HMI observations and the SGK pipeline (black dots, purple circles and magenta circles respectively). The solid and dashed vertical lines mark respectively the positions of solar maxima and solar minima.

derived positions during cycle 25 are near mirror-image of the values during the declining phase of cycle 24, like the jump, is more difficult to discern, though it appears to be so. As noticed before by (Antia & Basu 2022; Basu & Korzennik 2024), the results derived from GONG and HMI observations agree better than those derived from GONG and MDI observations.

The scatter in the results for the width of the tachocline, w_d, is also quite large. Consequently, while it appears that the temporal trend during cycle 23 was different, we cannot ascertain whether they are statistically significant. However, we do note that the official pipeline and SGK results are in quite good agreement.

4.2. *Results from longer time series data*

Since the data derived from the ≈ 1-year time series are quite noisy, we determined the tachocline parameters from longer time series data, although, we lose temporal resolution.

Even though the jump results are clearly significant even for results obtained with short time series data sets, for the sake of completeness, we show the result for jump using longer time series data sets in Fig. 4. These results are also presented in Tables 6, 7, 8 and 9. The general temporal variability is the same for all the data sets, but the change becomes smoother as the length of

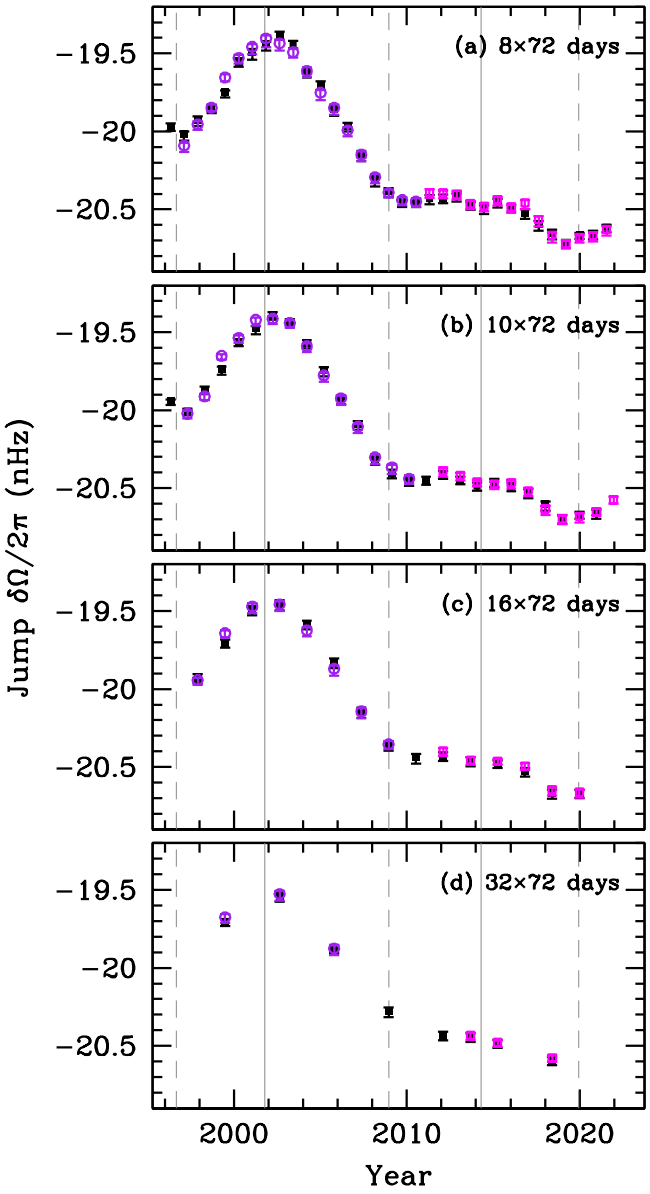

Figure 4. The jump in the rotation rate across the tachocline for data sets corresponding to the approximately 1.5-year, 2-year, 3-year and 6-year long time series data sets for GONG, MDI or HMI and the SGK pipeline. Like in Fig. 3, the black dots correspond to the GONG results, purple circles to MDI results and magenta circles to HMI results. The vertical solid and dashes lines mark epochs of solar maxima and minima, respectively.

the analyzed time series increases. The longer time series decreases the temporal resolution of the data. This causes time variations on scales shorter than the length of the time series to be averaged out. This averaging also decreases the amplitude of the variations

The estimated positions and widths of the tachocline are shown as a function of time in Fig. 5 for the different

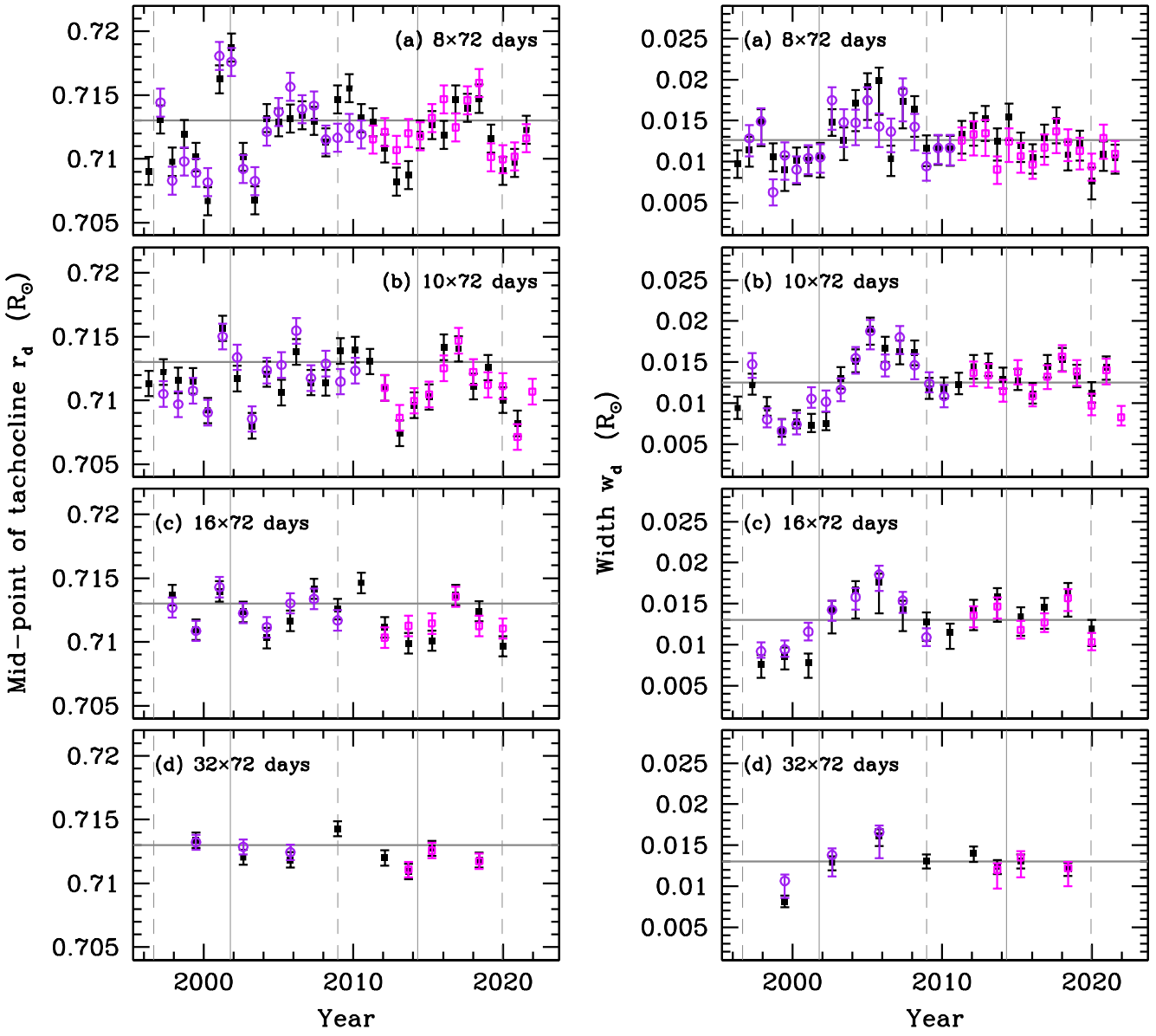

Figure 5. The position (left panels) and the width (right panels) of the tachocline plotted as a function of time for data sets of different time series length, i.e., $8\times, 10\times, 16\times$ and 32×72-day (top to bottom) and the SGK pipeline. Like in Fig. 3, the black dots correspond to the GONG results, purple circles to MDI results and magenta circles to HMI results. The vertical solid and dashes lines mark epochs of solar maxima and minima, respectively. The horizontal line in the panels on the left mark the position of the CZ base. The horizontal lines in the panels on the right are an average of all the points in each panel.

instruments. There was a statistically significant change in the position of the mid-point of the tachocline in solar cycle 24, which seems to be continuing in solar cycle 25. The issue is more confusing when looking at cycle 23. Indeed, the 8×72-day and the 10×72-day long results show a sudden change sometime before 2002. Since this change is seen when using both GONG and MDI data sets, it is tempting to believe that this change is real and not a result of the fitting technique either, as can be seen from Fig. 9(b). Such a change is also seen in results derived from the 5×72-day long data sets (see Fig. 2), but those have much larger uncertainties, and hence the sudden increase no longer stands out. Of course, this feature is smoothed out when longer time series data sets are used, thus, we cannot say with any certainty whether there was a sudden change in the tachocline position around 2001-2002.

As hinted by results obtained with the data sets corresponding to the 5×72-day long time series, there is a time variation in the width of the tachocline which is

best seen when using the 10×72-day long time series data sets — results derived from shorter time series are noisy, while results corresponding to longer ones tend to average out a lot of the variation. As can be seen from Fig. 5, the variations of the width during cycle 23 were very different from the variations during cycle 24 which are not statistically significant.

5. DISCUSSION

We have determined tachocline parameters from helioseismic mode splittings obtained with various lengths of time series. This allows us to beat down the noise in the analysis in order to examine whether the position of the mid-point of the tachocline and its thickness vary with time.

Basu & Antia (2019) has already shown that the jump in the rotation rate changes with time. This work confirms that, and extends the results to the ascending phase of solar cycle 25. The change during cycle 25 seems to be a mirror image of the change during the descending phase of cycle 24. This leads us to speculate that there could be a longer magnetic cycle present at the tachocline. We need to wait for additional data acquired beyond cycle-25, namely during the ascending part of cycle 26, to confirm this.

We find that both the position, and the width of the tachocline change with time. The results are statistically significant only for some epochs — for instance, the width changed considerably during solar cycle 23, but less so during cycle 24. The opposite is true for the change in the position of the tachocline — the results for cycle 23 are confusing, but there is a clear signature of change in cycle 24. During cycle 24, the tachocline was deeper in the radiative zone just before the maximum, then moved closer to the convection zone in the middle of the descending phase, and started going deeper again.

Given that both the position and the width of the tachocline vary with time, it is instructive to look at the upper and lower boundaries of the tachocline, i.e., $r_d + w_d$ and $r_d - wd$ as is shown in Fig. 6; recall that this region spans the radius range where the rotation rate changes from $0.269\,\delta\Omega$ to $0.731\,\delta\Omega$. While this information is available in Fig. 5, this representation offers a better visualization of the changes. If we look at the results derived from the two intermediate-length time series, i.e., the 10×72-day and 16×72-day long ones, it appears that the tachocline becomes narrower around the time of solar maximum. The extent increases after the maximum and starts decreasing again. Since the maximum of solar cycle 25 is imminent, another a few more years of helioseismic data should be able to show whether this is indeed the case, or whether noise in the results is fooling us.

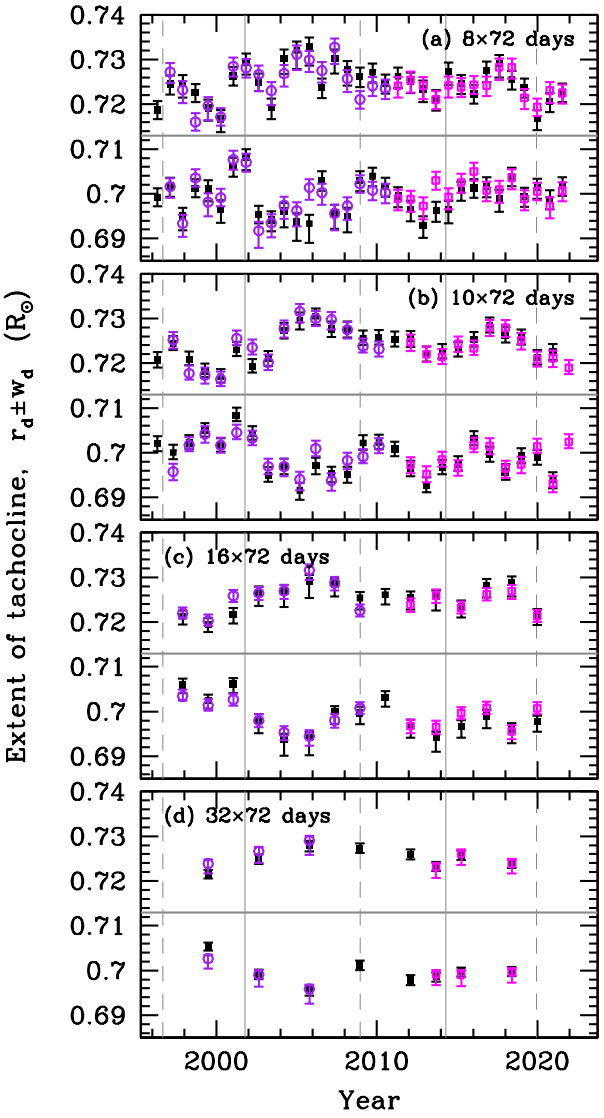

Figure 6. The upper and lower boundaries of the tachocline, i.e., $r_d + w_d$ and $r_d - w_d$, plotted as a function of time for data sets obtained with different time series lengths, i.e., $8\times, 10\times, 16\times$ and 32×72-day (top to bottom) and the SGK pipeline. Like in Fig. 3, the black dots correspond to the GONG results, purple circles to MDI results and magenta circles to HMI results. The vertical solid and dashes lines mark epochs of solar maxima and minima, respectively. The horizontal line marks the position of the CZ base.

Our results reinforce the need to continue helioseismic monitoring of the Sun to understand solar activity and its evolution.

ACKNOWLEDGEMENTS

This work is supported by NASA grant 80NSSC23K0563 to SB. and NASA grants

80NSSC22K0516 and NNH18ZDA001N-DRIVE to SGK. This work utilizes data from the National Solar Observatory Integrated Synoptic Program, which is operated by the Association of Universities for Research in Astronomy, under a cooperative agreement with the National Science Foundation and with additional financial support from the National Oceanic and Atmospheric Administration, the National Aeronautics and Space Administration, and the United States Air Force. The GONG network of instruments is hosted by the Big Bear Solar Observatory, High Altitude Observatory, Learmonth Solar Observatory, Udaipur Solar Observatory, Instituto de Astrofísica de Canarias, and Cerro Tololo Interamerican Observatory. This work also uses provided by the SOHO/MDI consortium. SOHO is a project of international cooperation between ESA and NASA. We also use data from the Helioseismic and Magnetic Imager on board the Solar Dynamics Observatory. HMI data are courtesy of NASA/SDO and the AIA, EVE, and HMI science teams.

Facilities: GONG, MDI, HMI, Royal Observatory of Belgium, Brussels

REFERENCES

Aguirre Børsen-Koch, V., Rørsted, J. L., Justesen, A. B., et al. 2022, MNRAS, 509, 4344, doi: 10.1093/mnras/stab2911

Antia, H. M., & Basu, S. 2011, ApJL, 735, L45, doi: 10.1088/2041-8205/735/2/L45

—. 2022, ApJ, 924, 19, doi: 10.3847/1538-4357/ac32c3

Antia, H. M., Basu, S., & Chitre, S. M. 1998, MNRAS, 298, 543, doi: 10.1046/j.1365-8711.1998.01635.x

Basu, S. 1997, MNRAS, 288, 572, doi: 10.1093/mnras/288.3.572

Basu, S., & Antia, H. M. 2019, ApJ, 883, 93, doi: 10.3847/1538-4357/ab3b57

Basu, S., & Korzennik, S. G. 2024, ApJ, 964, 8, doi: 10.3847/1538-4357/ad2203

Charbonneau, P., Christensen-Dalsgaard, J., Henning, R., et al. 1999, ApJ, 527, 445, doi: 10.1086/308050

Chatterjee, P., Nandy, D., & Choudhuri, A. R. 2004, A&A, 427, 1019, doi: 10.1051/0004-6361:20041199

de Jager, C., Akasofu, S. I., Duhau, S., et al. 2016, SSRv, 201, 109, doi: 10.1007/s11214-016-0293-9

Dikpati, M., & Charbonneau, P. 1999, ApJ, 518, 508, doi: 10.1086/307269

Dikpati, M., & Gilman, P. A. 2001, ApJ, 552, 348, doi: 10.1086/320446

Gai, N., Basu, S., Chaplin, W. J., & Elsworth, Y. 2011, ApJ, 730, 63, doi: 10.1088/0004-637X/730/2/63

Guerrero, G., & de Gouveia Dal Pino, E. M. 2008, A&A, 485, 267, doi: 10.1051/0004-6361:200809351

Guerrero, G., Smolarkiewicz, P. K., de Gouveia Dal Pino, E. M., Kosovichev, A. G., & Mansour, N. N. 2016, ApJ, 819, 104, doi: 10.3847/0004-637X/819/2/104

Guerrero, G., Smolarkiewicz, P. K., de Gouveia Dal Pino, E. M., et al. 2017, in Living Around Active Stars, ed. D. Nandy, A. Valio, & P. Petit, Vol. 328, 61–68, doi: 10.1017/S1743921317003982

Hill, F., Stark, P. B., Stebbins, R. T., et al. 1996, Science, 272, 1292

Joe, S., & Kuo, F. Y. 2003, ACM Transactions on Mathematical Software, 29, 49, doi: doi.org/10.1145/641876.6418

Joe, S., & Kuo, F. Y. 2008, SIAM Journal on Scientific Computing, 30, 2635, doi: 10.1137/070709359

Korzennik, S. G. 2004, in ESA Special Publication, Vol. 559, SOHO 14 Helio- and Asteroseismology: Towards a Golden Future, ed. D. Danesy, 524. https://arxiv.org/abs/astro-ph/0406470

Korzennik, S. G. 2008a, Astronomische Nachrichten, 329, 453, doi: 10.1002/asna.200710979

Korzennik, S. G. 2008b, in Journal of Physics Conference Series, Vol. 118, Journal of Physics Conference Series, 012082, doi: 10.1088/1742-6596/118/1/012082

Korzennik, S. G. 2017, in AAS/Solar Physics Division Meeting, Vol. 48, AAS/Solar Physics Division Abstracts #48, 113.02

Korzennik, S. G. 2018, in Catalyzing Solar Connections, 132

—. 2023, Frontiers in Astronomy and Space Sciences, 9, 1031313, doi: 10.3389/fspas.2022.1031313

Korzennik, S. G., & Eff-Darwich, A. 2013, in Journal of Physics Conference Series, Vol. 440, Journal of Physics Conference Series, 012015, doi: 10.1088/1742-6596/440/1/012015

Kosovichev, A. G. 1996, ApJL, 469, L61, doi: 10.1086/310253

Press, W. H., Teukolsky, S. A., Vetterling, W. T., & Flannery, B. P. 1992, Numerical recipes in FORTRAN. The art of scientific computing (Cambridge University Press)

Ritzwoller, M. H., & Lavely, E. M. 1991, ApJ, 369, 557, doi: 10.1086/169785

Scherrer, P. H., Bogart, R. S., Bush, R. I., et al. 1995, SoPh, 162, 129

Scherrer, P. H., Schou, J., Bush, R. I., et al. 2012, SoPh, 275, 207

Schou, J., Antia, H. M., Basu, S., et al. 1998, ApJ, 505, 390, doi: 10.1086/306146

Schou, J., Howe, R., Basu, S., et al. 2002, ApJ, 567, 1234, doi: 10.1086/338665

Sobol, I. M. 1967, USSR Computational Mathematics and Mathematical Physics, 7, 86, doi: 10.1016/0041-5553(67)90144-9

Stello, D., Chaplin, W. J., Bruntt, H., et al. 2009, ApJ, 700, 1589, doi: 10.1088/0004-637X/700/2/1589

Vanderbilt, D., & Louie, S. G. 1984, Journal of Computational Physics, 56, 259, doi: 10.1016/0021-9991(84)90095-0

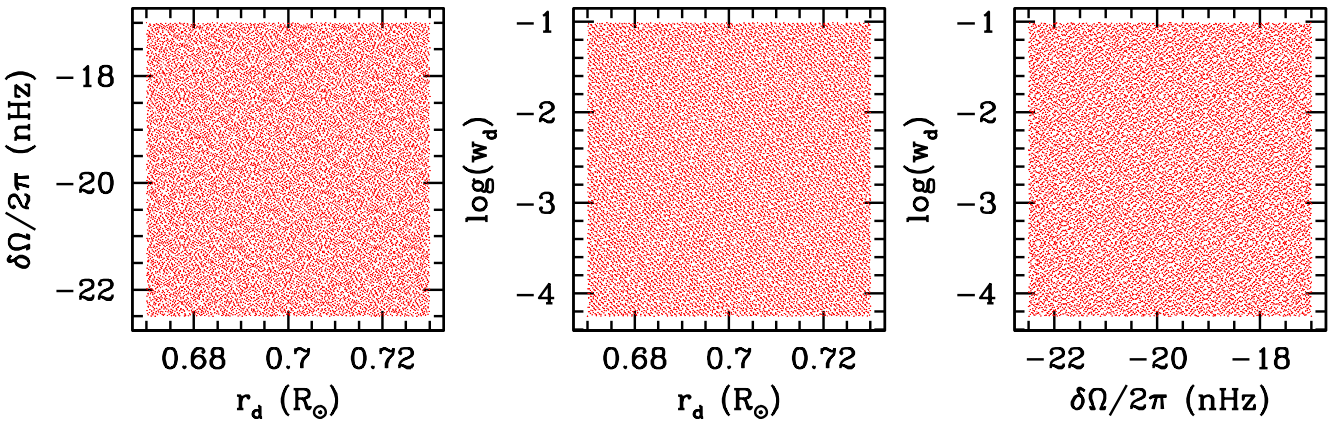

Figure 7. The distribution of tachocline parameters in the grid of 15000 models.

APPENDIX

A. FITTING METHODS

We considered two different forward modeling techniques to derive the three parameters that characterize our representation of the tachocline. The first is simply a search on a pre-computed grid of models, inspired by techniques used in asteroseismology (e.g., Stello et al. 2009; Gai et al. 2011; Aguirre Børsen-Koch et al. 2022), while the second is a simulated annealing minimization.

A.1. *Grid-based fitting*

For the grid-based fitting method, we calculate the c_3 splitting coefficients of models with different combinations of r_d, $\Delta\Omega$ and w_d. The parameters are distributed in a 3D Sobol sequence (Sobol 1967) of length 15000 to ensure uniformity of coverage of the three-dimensional parameter space. We use the code from Joe & Kuo (2003); Joe & Kuo (2008)[2] to determine the Sobol numbers. The coverage of the parameters is shown in Fig. 7; note that since the width of the tachocline is small (Antia et al. 1998; Antia & Basu 2011), we choose a distribution of $\log(w_d)$ rather than w_d.

We follow the method proposed for Gai et al. (2011), namely for each model, we calculate the χ^2 between the observed and model splittings. The χ^2, assuming a Gaussian distribution of errors, can be converted to a likelihood for each model as follows:

$$\mathcal{L}_i = \frac{\exp(-\chi^2/2)}{\sum_{i=1}^{N} \exp(-\chi^2/2)}, \tag{A1}$$

where N is the total number of models. The parameters of the tachocline are determined by averaging the parameters of the models with likelihood $\mathcal{L} \geq 0.90\,\mathcal{L}_{\rm max}$, where $\mathcal{L}_{\rm max}$ is the maximum likelihood obtained. The uncertainties are determined using a traditional bootstrapping method of simulating many realizations of the observations, fit each one of them in exactly the same manner as the original data and use the spread as a measure of uncertainty.

A.2. *Simulated annealing*

We use simulated annealing (hereafter SA; Vanderbilt & Louie 1984; Press et al. 1992) to minimize the χ^2 between computed and observed values of c_3. This algorithm uses randomly generated values of the parameters, and we assume that the parameters have Gaussian priors with the mean and width of the Gaussian determined from existing inversions of rotational splittings. These inversions have clearly shown the presence of a tachocline, but do not fully resolve it,

[2] https://web.maths.unsw.edu.au/ fkuo/sobol/

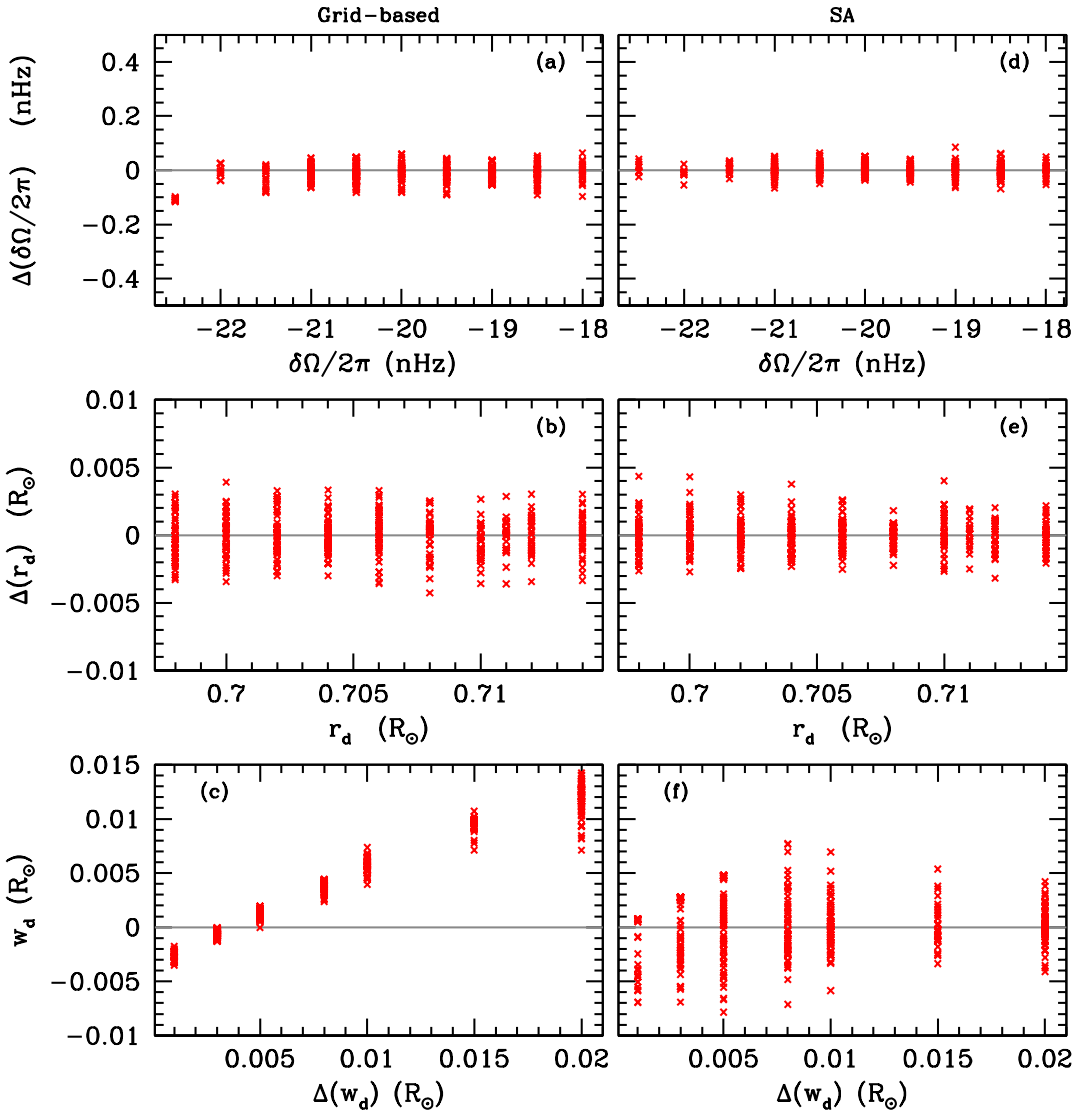

Figure 8. The difference between the exact and estimated values of tachocline properties plotted as a function of the exact value of the parameters. The differences are in the sense (Exact − Estimate). The left-hand panels (a, b, and c) show results for the grid-based method, the right-hand panels (d, e, and f) show results from simulated annealing.

since regularization is achieved via some form of smoothing. Given that there is a chance that the solution becomes trapped in a local minimum, we make 80 different attempts using different sequences of randomly selected initial guesses in order to derive a global χ^2 minimum. We can be certain that the algorithm reached a global minimum by inspecting the likelihood weighted distribution of all the parameters for all iterations, where the likelihood is defined as $\exp(-\chi^2/2)$. Indeed, when a global minimum has been reached the distribution is single peaked, otherwise it will have multiple peaks. We found that $\delta\Omega$ is the first parameter to converge, followed by r_d; w_d takes the longest to converge. As with the grid based case, we determine the uncertainties using a bootstrapping method. Earlier works (Antia et al. 1998; Antia & Basu 2011; Basu & Antia 2019) used the same approach.

A.3. *Comparison*

Test results obtained with the grid and SA methods are presented in Fig. 8, where we show results obtained for models with known tachocline properties; we included uncertainties that correspond to those for a 10×72-day long HMI data set.

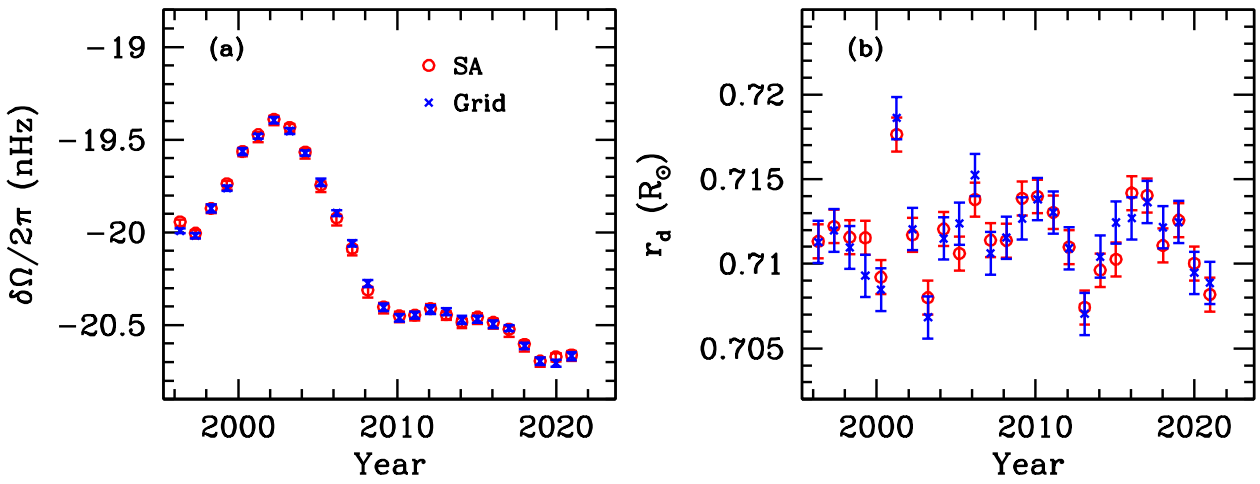

Figure 9. Estimates of r_d and $\Delta\Omega$ for different sets of GONG splittings obtained with 10×72-day long time series.

The figure shows clearly that both the grid-based and simulated annealing methods perform rather well for the jump, $\Delta\Omega$, and the position, r_d, parameters. The resulting spread is consistent with the uncertainties obtained by bootstrapping. The one notable exception are the grid-based results for models with the largest jump amplitude, $|\delta\Omega|$; this can be attributed to the fact that these models fall at the edge of our Sobol distribution, and hence the resulting truncation causes a systematic error. Results obtained for the width parameter, w_d, are not as good. The SA results show a systematic error at very low values, i.e., the thickness is generally overestimated in those cases, the results are good for larger w_d. In contrast, the grid-based method does very poorly overall: it overestimates the width at the low end, and underestimates it at the high end.

Since one of the aims of this work is to determine possible changes in width, w_d, we cannot use a method that has width-dependent systematic errors. Hence, we show only results obtained with the SA method. As shown in Fig. 9, the values of r_d and $\delta\Omega$ obtained by the two methods are commensurate with each other, suggesting that we could cut down on computational time by determining r_d and $\delta\Omega$ using the grid-based method but use the SA method, keeping r_d and $\delta\Omega$ fixed, to derive the width, w_d, however, we chose not to do so.

B. TABLES WITH RESULTS

This Appendix lists all our results. Note that once the analyzed time series becomes long enough, the uncertainties in the tachocline parameters become symmetric. The start date of each set has the format YYYYMMDD.

Table 1. Jump of the tachocline from 72-day GONG SGK sets

Start Date	$\delta\Omega/2pi$ (nHz)	Start Date	$\delta\Omega/2\pi$ (nHz)	Start Date	$\delta\Omega/2\pi$ (nHz)
19950507	$-19.8566^{+0.0182}_{-0.0516}$	20041022	$-19.6214^{+0.0241}_{-0.0357}$	20140409	$-20.4649^{+0.0197}_{-0.0586}$
19950718	$-19.6371^{+0.0236}_{-0.0438}$	20050102	$-19.5886^{+0.0383}_{-0.0245}$	20140620	$-20.7384^{+0.0392}_{-0.0217}$
19950928	$-20.0472^{+0.0360}_{-0.0260}$	20050315	$-19.7492^{+0.0257}_{-0.0410}$	20140831	$-20.4938^{+0.0237}_{-0.0466}$
19951209	$-20.0563^{+0.0248}_{-0.0521}$	20050526	$-19.8756^{+0.0170}_{-0.0373}$	20141111	$-20.5675^{+0.0254}_{-0.0513}$
19960219	$-20.0845^{+0.0395}_{-0.0354}$	20050806	$-19.7622^{+0.0244}_{-0.0459}$	20150122	$-20.5999^{+0.0265}_{-0.0749}$
19960501	$-20.1331^{+0.0197}_{-0.0479}$	20051017	$-20.0683^{+0.0228}_{-0.0483}$	20150404	$-20.4176^{+0.0181}_{-0.0486}$
19960712	$-19.9316^{+0.0186}_{-0.0550}$	20051228	$-19.9863^{+0.0261}_{-0.0425}$	20150615	$-20.7548^{+0.0344}_{-0.0368}$
19960922	$-20.1155^{+0.0186}_{-0.0437}$	20060310	$-20.0248^{+0.0241}_{-0.0624}$	20150826	$-20.7176^{+0.0275}_{-0.0452}$
19961203	$-20.0723^{+0.0229}_{-0.0377}$	20060521	$-19.9696^{+0.0253}_{-0.0342}$	20151106	$-20.4667^{+0.0276}_{-0.0536}$
19970213	$-20.2053^{+0.0224}_{-0.0457}$	20060801	$-19.9332^{+0.0263}_{-0.0370}$	20160117	$-20.6676^{+0.0456}_{-0.0211}$
19970426	$-19.9582^{+0.0303}_{-0.0244}$	20061012	$-20.1746^{+0.0207}_{-0.0670}$	20160329	$-20.4049^{+0.0186}_{-0.0433}$
19970707	$-19.8830^{+0.0300}_{-0.0294}$	20061223	$-20.2540^{+0.0431}_{-0.0365}$	20160609	$-20.6393^{+0.0181}_{-0.0458}$
19970917	$-19.8936^{+0.0260}_{-0.0412}$	20070305	$-20.1287^{+0.0315}_{-0.0276}$	20160820	$-20.4980^{+0.0163}_{-0.0444}$
19971128	$-19.9900^{+0.0389}_{-0.0264}$	20070516	$-20.2068^{+0.0133}_{-0.0530}$	20161031	$-20.7429^{+0.0328}_{-0.0185}$
19980208	$-19.8379^{+0.0242}_{-0.0265}$	20070727	$-20.0463^{+0.0269}_{-0.0362}$	20170111	$-20.4750^{+0.0331}_{-0.0221}$
19980421	$-20.0556^{+0.0239}_{-0.0434}$	20071007	$-20.3816^{+0.0239}_{-0.0579}$	20170324	$-20.4308^{+0.0217}_{-0.0452}$
19980702	$-19.8401^{+0.0252}_{-0.0506}$	20071218	$-20.2992^{+0.0229}_{-0.0435}$	20170604	$-20.6197^{+0.0268}_{-0.0349}$
19980912	$-19.8781^{+0.0592}_{-0.0139}$	20080228	$-20.3299^{+0.0167}_{-0.0367}$	20170815	$-20.6068^{+0.0247}_{-0.0448}$
19981123	$-20.0083^{+0.0195}_{-0.0493}$	20080510	$-20.6472^{+0.0153}_{-0.0537}$	20171026	$-20.7810^{+0.0298}_{-0.0440}$
19990203	$-19.9036^{+0.0241}_{-0.0262}$	20080721	$-20.2549^{+0.0307}_{-0.0411}$	20180106	$-20.6637^{+0.0245}_{-0.0623}$
19990416	$-20.0641^{+0.0357}_{-0.0373}$	20081001	$-20.4995^{+0.0246}_{-0.0467}$	20180319	$-20.8212^{+0.0354}_{-0.0452}$
19990627	$-19.4271^{+0.0196}_{-0.0427}$	20081212	$-20.3891^{+0.0227}_{-0.0432}$	20180530	$-21.0173^{+0.0246}_{-0.0612}$
19990907	$-19.6132^{+0.0286}_{-0.0198}$	20090222	$-20.4555^{+0.0225}_{-0.0504}$	20180810	$-20.6874^{+0.0203}_{-0.0413}$
19991118	$-19.5654^{+0.0295}_{-0.0304}$	20090505	$-20.6328^{+0.0232}_{-0.0562}$	20181021	$-20.7643^{+0.0218}_{-0.0456}$
20000129	$-19.7519^{+0.0290}_{-0.0403}$	20090716	$-20.6521^{+0.0259}_{-0.0425}$	20190101	$-20.8043^{+0.0292}_{-0.0495}$
20000410	$-19.8486^{+0.0191}_{-0.0469}$	20090926	$-20.5207^{+0.0235}_{-0.0600}$	20190314	$-20.7933^{+0.0228}_{-0.0340}$
20000621	$-19.5918^{+0.0202}_{-0.0475}$	20091207	$-20.6024^{+0.0191}_{-0.0482}$	20190525	$-20.7522^{+0.0324}_{-0.0269}$
20000901	$-19.4279^{+0.0326}_{-0.0414}$	20100217	$-20.4904^{+0.0264}_{-0.0483}$	20190805	$-20.7280^{+0.0318}_{-0.0405}$
20001112	$-19.6029^{+0.0401}_{-0.0184}$	20100430	$-20.6367^{+0.0256}_{-0.0464}$	20191016	$-20.8537^{+0.0290}_{-0.0354}$
20010123	$-19.6732^{+0.0219}_{-0.0422}$	20100711	$-20.6044^{+0.0242}_{-0.0451}$	20191227	$-20.6676^{+0.0234}_{-0.0326}$
20010405	$-19.5361^{+0.0263}_{-0.0579}$	20100921	$-20.6101^{+0.0353}_{-0.0354}$	20200308	$-20.8929^{+0.0351}_{-0.0261}$
20010616	$-19.4317^{+0.0186}_{-0.0496}$	20101202	$-20.6297^{+0.0184}_{-0.0472}$	20200519	$-20.9001^{+0.0302}_{-0.0258}$
20010827	$-19.4963^{+0.0233}_{-0.0626}$	20110212	$-20.3637^{+0.0321}_{-0.0278}$	20200730	$-20.6604^{+0.0241}_{-0.0508}$
20011107	$-19.4978^{+0.0207}_{-0.0566}$	20110425	$-20.5442^{+0.0195}_{-0.0464}$	20201010	$-20.9621^{+0.0308}_{-0.0342}$
20020118	$-19.2549^{+0.0271}_{-0.0323}$	20110706	$-20.2877^{+0.0278}_{-0.0326}$	20201221	$-20.9010^{+0.0229}_{-0.0650}$
20020331	$-19.4435^{+0.0261}_{-0.0573}$	20110916	$-20.6209^{+0.0235}_{-0.0263}$	20210303	$-20.5756^{+0.0249}_{-0.0338}$
20020611	$-19.6054^{+0.0429}_{-0.0236}$	20111127	$-20.3426^{+0.0149}_{-0.0528}$	20210514	$-20.6159^{+0.0200}_{-0.0261}$
20020822	$-19.5739^{+0.0291}_{-0.0452}$	20120207	$-20.4259^{+0.0500}_{-0.0229}$	20210725	$-20.7356^{+0.0191}_{-0.0465}$
20021102	$-19.6470^{+0.0270}_{-0.0186}$	20120419	$-20.2485^{+0.0284}_{-0.0366}$	20211005	$-20.7501^{+0.0241}_{-0.0492}$
20030113	$-19.4773^{+0.0270}_{-0.0296}$	20120630	$-20.4569^{+0.0279}_{-0.0254}$	20211216	$-20.6728^{+0.0167}_{-0.0460}$
20030326	$-19.4735^{+0.0247}_{-0.0537}$	20120910	$-20.4248^{+0.0191}_{-0.0502}$	20220226	$-20.4064^{+0.0165}_{-0.0400}$
20030606	$-19.4488^{+0.0321}_{-0.0269}$	20121121	$-20.6339^{+0.0198}_{-0.0442}$	20220509	$-20.5813^{+0.0274}_{-0.0377}$
20030817	$-19.7385^{+0.0206}_{-0.0476}$	20130201	$-20.3595^{+0.0294}_{-0.0213}$	20220720	$-20.6968^{+0.0131}_{-0.0493}$
20031028	$-19.5246^{+0.0250}_{-0.0510}$	20130414	$-20.5101^{+0.0173}_{-0.0544}$	20220930	$-20.5550^{+0.0236}_{-0.0328}$
20040108	$-19.5464^{+0.0256}_{-0.0289}$	20130625	$-20.6132^{+0.0374}_{-0.0482}$	20221211	$-20.7301^{+0.0304}_{-0.0476}$
20040320	$-19.6202^{+0.0214}_{-0.0406}$	20130905	$-20.5644^{+0.0239}_{-0.0429}$	20230221	$-20.4651^{+0.0188}_{-0.0353}$
20040531	$-19.7432^{+0.0487}_{-0.0144}$	20131116	$-20.6504^{+0.0202}_{-0.0492}$	20230504	$-20.7537^{+0.0271}_{-0.0428}$
20040811	$-19.7935^{+0.0450}_{-0.0142}$	20140127	$-20.4498^{+0.0182}_{-0.0418}$	20230715	$-20.3922^{+0.0264}_{-0.0266}$

Table 2. Jump of the tachocline from 72-day MDI SGK sets

Start Date	$\delta\Omega/2\pi$ (nHz)	Start Date	$\delta\Omega/2\pi$ (nHz)	Start Date	$\delta\Omega/2\pi$ (nHz)
19960501	$-20.2503^{+0.0015}_{-0.0062}$	20010827	$-19.5587^{+0.0021}_{-0.0050}$	20060801	$-20.0478^{+0.0042}_{-0.0023}$
19960712	$-20.1691^{+0.0017}_{-0.0059}$	20011107	$-19.3168^{+0.0020}_{-0.0063}$	20061012	$-20.1769^{+0.0019}_{-0.0043}$
19960922	$-20.1874^{+0.0028}_{-0.0042}$	20020118	$-19.4403^{+0.0028}_{-0.0029}$	20061223	$-20.1697^{+0.0035}_{-0.0050}$
19961203	$-20.0857^{+0.0019}_{-0.0043}$	20020331	$-19.5229^{+0.0020}_{-0.0058}$	20070305	$-20.2580^{+0.0033}_{-0.0049}$
19970213	$-20.1462^{+0.0027}_{-0.0069}$	20020611	$-19.5605^{+0.0019}_{-0.0043}$	20070516	$-20.4187^{+0.0026}_{-0.0048}$
19970426	$-19.9723^{+0.0036}_{-0.0034}$	20020822	$-19.6077^{+0.0033}_{-0.0014}$	20070727	$-20.2798^{+0.0028}_{-0.0042}$
19970707	$-20.0902^{+0.0020}_{-0.0046}$	20021102	$-19.6186^{+0.0026}_{-0.0049}$	20071007	$-20.3782^{+0.0030}_{-0.0061}$
19970917	$-20.1766^{+0.0018}_{-0.0043}$	20030113	$-19.6110^{+0.0029}_{-0.0033}$	20071218	$-20.3600^{+0.0022}_{-0.0060}$
19971128	$-20.0585^{+0.0017}_{-0.0044}$	20030326	$-19.6749^{+0.0019}_{-0.0061}$	20080228	$-20.1351^{+0.0028}_{-0.0038}$
19980208	$-20.1481^{+0.0024}_{-0.0041}$	20030606	$-19.8136^{+0.0030}_{-0.0016}$	20080510	$-20.6669^{+0.0033}_{-0.0058}$
19980421	$-20.0007^{+0.0030}_{-0.0031}$	20030817	$-19.5407^{+0.0028}_{-0.0025}$	20080721	$-20.3907^{+0.0023}_{-0.0038}$
19981018	$-20.0126^{+0.0019}_{-0.0036}$	20031028	$-19.5741^{+0.0026}_{-0.0063}$	20081001	$-20.5772^{+0.0024}_{-0.0056}$
19990203	$-19.9554^{+0.0030}_{-0.0028}$	20040108	$-19.6901^{+0.0028}_{-0.0033}$	20081212	$-20.5829^{+0.0015}_{-0.0063}$
19990416	$-19.7884^{+0.0019}_{-0.0049}$	20040320	$-19.8040^{+0.0021}_{-0.0017}$	20090222	$-20.4640^{+0.0035}_{-0.0031}$
19990627	$-19.7345^{+0.0026}_{-0.0037}$	20040531	$-19.8189^{+0.0024}_{-0.0044}$	20090505	$-20.5958^{+0.0018}_{-0.0058}$
19990907	$-19.7868^{+0.0037}_{-0.0029}$	20040811	$-19.7326^{+0.0042}_{-0.0031}$	20090716	$-20.7213^{+0.0025}_{-0.0074}$
19991118	$-19.6946^{+0.0048}_{-0.0017}$	20041022	$-19.6671^{+0.0022}_{-0.0034}$	20090926	$-20.5295^{+0.0022}_{-0.0055}$
20000129	$-19.7874^{+0.0025}_{-0.0042}$	20050102	$-19.6293^{+0.0028}_{-0.0020}$	20091207	$-20.6988^{+0.0027}_{-0.0060}$
20000410	$-19.9058^{+0.0023}_{-0.0073}$	20050315	$-19.8877^{+0.0036}_{-0.0035}$	20100217	$-20.5776^{+0.0040}_{-0.0037}$
20000621	$-19.5964^{+0.0025}_{-0.0053}$	20050526	$-19.8974^{+0.0025}_{-0.0061}$	20100430	$-20.5131^{+0.0027}_{-0.0039}$
20000901	$-19.5607^{+0.0048}_{-0.0030}$	20050806	$-19.7870^{+0.0022}_{-0.0043}$	20100711	$-20.6548^{+0.0023}_{-0.0062}$
20001112	$-19.4472^{+0.0063}_{-0.0021}$	20051017	$-19.9619^{+0.0031}_{-0.0034}$	20100921	$-20.5065^{+0.0028}_{-0.0044}$
20010123	$-19.5956^{+0.0030}_{-0.0044}$	20051228	$-20.0529^{+0.0043}_{-0.0021}$	20101202	$-20.5856^{+0.0020}_{-0.0037}$
20010405	$-19.4845^{+0.0024}_{-0.0051}$	20060310	$-19.9890^{+0.0026}_{-0.0043}$	20110212	$-20.3828^{+0.0030}_{-0.0026}$
20010616	$-19.2273^{+0.0022}_{-0.0040}$	20060521	$-20.0779^{+0.0029}_{-0.0043}$		

Table 3. Jump of the tachocline from 72-day HMI SGK sets

Start Date	$\delta\Omega/2\pi$ (nHz)	Start Date	$\delta\Omega/2\pi$ (nHz)	Start Date	$\delta\Omega/2\pi$ (nHz)
20100430	$-20.4498^{+0.0028}_{-0.0039}$	20141111	$-20.7100^{+0.0039}_{-0.0046}$	20190525	$-20.7434^{+0.0025}_{-0.0041}$
20100711	$-20.5844^{+0.0028}_{-0.0052}$	20150122	$-20.4783^{+0.0024}_{-0.0038}$	20190805	$-20.8289^{+0.0022}_{-0.0068}$
20100921	$-20.6022^{+0.0027}_{-0.0052}$	20150404	$-20.4555^{+0.0015}_{-0.0055}$	20191016	$-20.7255^{+0.0026}_{-0.0012}$
20101202	$-20.4409^{+0.0021}_{-0.0051}$	20150615	$-20.5713^{+0.0024}_{-0.0017}$	20191227	$-20.7754^{+0.0027}_{-0.0034}$
20110212	$-20.4206^{+0.0027}_{-0.0041}$	20150826	$-20.4761^{+0.0018}_{-0.0034}$	20200308	$-20.7407^{+0.0018}_{-0.0054}$
20110425	$-20.5224^{+0.0021}_{-0.0034}$	20151106	$-20.4497^{+0.0016}_{-0.0044}$	20200519	$-20.8810^{+0.0020}_{-0.0030}$
20110706	$-20.3857^{+0.0022}_{-0.0035}$	20160117	$-20.6674^{+0.0033}_{-0.0017}$	20200730	$-20.7100^{+0.0019}_{-0.0041}$
20110916	$-20.6772^{+0.0020}_{-0.0040}$	20160329	$-20.5105^{+0.0031}_{-0.0040}$	20201010	$-20.8076^{+0.0028}_{-0.0041}$
20111127	$-20.4321^{+0.0013}_{-0.0062}$	20160609	$-20.6177^{+0.0027}_{-0.0037}$	20201221	$-20.9688^{+0.0024}_{-0.0053}$
20120207	$-20.5094^{+0.0030}_{-0.0019}$	20160820	$-20.4964^{+0.0014}_{-0.0041}$	20210303	$-20.6134^{+0.0028}_{-0.0035}$
20120419	$-20.3798^{+0.0032}_{-0.0037}$	20161031	$-20.7282^{+0.0020}_{-0.0025}$	20210514	$-20.5174^{+0.0025}_{-0.0025}$
20120630	$-20.3790^{+0.0024}_{-0.0032}$	20170111	$-20.8570^{+0.0045}_{-0.0017}$	20210725	$-20.7672^{+0.0024}_{-0.0046}$
20120910	$-20.6365^{+0.0017}_{-0.0072}$	20170324	$-20.6227^{+0.0027}_{-0.0063}$	20211005	$-20.5307^{+0.0031}_{-0.0030}$
20121121	$-20.5828^{+0.0019}_{-0.0041}$	20170604	$-20.4970^{+0.0018}_{-0.0052}$	20211216	$-20.7353^{+0.0025}_{-0.0042}$
20130201	$-20.4643^{+0.0015}_{-0.0036}$	20170815	$-20.5485^{+0.0027}_{-0.0047}$	20220226	$-20.4623^{+0.0018}_{-0.0061}$
20130414	$-20.5391^{+0.0022}_{-0.0040}$	20171026	$-20.6194^{+0.0027}_{-0.0044}$	20220509	$-20.5587^{+0.0023}_{-0.0044}$
20130625	$-20.5374^{+0.0023}_{-0.0048}$	20180106	$-20.6183^{+0.0015}_{-0.0063}$	20220720	$-20.6872^{+0.0023}_{-0.0039}$
20130905	$-20.6662^{+0.0038}_{-0.0040}$	20180319	$-20.8412^{+0.0024}_{-0.0051}$	20220930	$-20.5170^{+0.0021}_{-0.0032}$
20131116	$-20.6551^{+0.0020}_{-0.0040}$	20180530	$-21.0651^{+0.0034}_{-0.0036}$	20221211	$-20.6180^{+0.0046}_{-0.0013}$
20140127	$-20.3976^{+0.0028}_{-0.0038}$	20180810	$-20.7766^{+0.0056}_{-0.0018}$	20230221	$-20.5612^{+0.0030}_{-0.0046}$
20140409	$-20.4271^{+0.0025}_{-0.0056}$	20181021	$-20.7087^{+0.0021}_{-0.0036}$	20230504	$-20.7661^{+0.0027}_{-0.0041}$
20140620	$-20.6925^{+0.0024}_{-0.0039}$	20190101	$-20.8338^{+0.0027}_{-0.0067}$	20230715	$-20.5102^{+0.0019}_{-0.0053}$
20140831	$-20.5169^{+0.0021}_{-0.0041}$	20190314	$-20.7321^{+0.0022}_{-0.0053}$		

Table 4. Tachocline properties from 5 × 72-day SGK sets

Start Date	$\delta\Omega/2\pi$ (nHz)	r_d ($R_\odot$)	w_d ($R_\odot$)	$\delta\Omega/2\pi$ (nHz)	r_d ($R_\odot$)	w_d ($R_\odot$)
	Asymmetric Fits			Symmetric Fits		
			GONG			
19950507	$-20.0690^{+0.0148}_{-0.0245}$	$0.7154^{+0.0007}_{-0.0017}$	$0.0037^{+0.0076}_{-0.0030}$	$-20.0654^{+0.0138}_{-0.0299}$	$0.7170^{+0.0007}_{-0.0015}$	$0.0050^{+0.0074}_{-0.0030}$
19960501	$-20.0673^{+0.0158}_{-0.0264}$	$0.7158^{+0.0007}_{-0.0017}$	$0.0036^{+0.0076}_{-0.0029}$	$-20.0654^{+0.0138}_{-0.0299}$	$0.7170^{+0.0007}_{-0.0015}$	$0.0080^{+0.0074}_{-0.0030}$
19970426	$-19.9135^{+0.0218}_{-0.0244}$	$0.7133^{+0.0012}_{-0.0019}$	$0.0116^{+0.0036}_{-0.0022}$	$-19.9322^{+0.0217}_{-0.0241}$	$0.7145^{+0.0013}_{-0.0019}$	$0.0127^{+0.0036}_{-0.0023}$
19980421	$-19.8334^{+0.0161}_{-0.0272}$	$0.7119^{+0.0011}_{-0.0018}$	$0.0084^{+0.0056}_{-0.0015}$	$-19.8347^{+0.0196}_{-0.0244}$	$0.7131^{+0.0011}_{-0.0020}$	$0.0088^{+0.0054}_{-0.0016}$
19990416	$-19.6066^{+0.0213}_{-0.0075}$	$0.7092^{+0.0008}_{-0.0017}$	$0.0079^{+0.0051}_{-0.0015}$	$-19.6106^{+0.0128}_{-0.0137}$	$0.7150^{+0.0006}_{-0.0016}$	$0.0086^{+0.0077}_{-0.0033}$
20000410	$-19.5624^{+0.0217}_{-0.0316}$	$0.7108^{+0.0015}_{-0.0018}$	$0.0158^{+0.0027}_{-0.0031}$	$-19.5636^{+0.0169}_{-0.0277}$	$0.7150^{+0.0013}_{-0.0021}$	$0.0114^{+0.0046}_{-0.0022}$
20010405	$-19.4357^{+0.0098}_{-0.0248}$	$0.7165^{+0.0006}_{-0.0016}$	$0.0045^{+0.0073}_{-0.0029}$	$-19.4228^{+0.0122}_{-0.0256}$	$0.7176^{+0.0006}_{-0.0017}$	$0.0083^{+0.0079}_{-0.0033}$
20020331	$-19.3976^{+0.0197}_{-0.0229}$	$0.7149^{+0.0014}_{-0.0019}$	$0.0160^{+0.0024}_{-0.0034}$	$-19.4112^{+0.0231}_{-0.0250}$	$0.7169^{+0.0015}_{-0.0019}$	$0.0168^{+0.0023}_{-0.0039}$
20030326	$-19.4451^{+0.0200}_{-0.0142}$	$0.7169^{+0.0011}_{-0.0020}$	$0.0104^{+0.0042}_{-0.0019}$	$-19.4826^{+0.0208}_{-0.0229}$	$0.7111^{+0.0012}_{-0.0019}$	$0.0147^{+0.0028}_{-0.0028}$
20040320	$-19.6017^{+0.0237}_{-0.0291}$	$0.7181^{+0.0017}_{-0.0019}$	$0.0179^{+0.0021}_{-0.0038}$	$-19.5992^{+0.0268}_{-0.0328}$	$0.7124^{+0.0017}_{-0.0019}$	$0.0173^{+0.0024}_{-0.0037}$
20050315	$-19.8881^{+0.0226}_{-0.0301}$	$0.7141^{+0.0015}_{-0.0018}$	$0.0191^{+0.0018}_{-0.0038}$	$-19.8531^{+0.0218}_{-0.0456}$	$0.7182^{+0.0014}_{-0.0021}$	$0.0139^{+0.0037}_{-0.0025}$
20060310	$-19.9554^{+0.0237}_{-0.0336}$	$0.7148^{+0.0012}_{-0.0020}$	$0.0120^{+0.0039}_{-0.0021}$	$-19.9800^{+0.0204}_{-0.0362}$	$0.7139^{+0.0014}_{-0.0019}$	$0.0136^{+0.0035}_{-0.0024}$
20070305	$-20.2511^{+0.0206}_{-0.0347}$	$0.7114^{+0.0015}_{-0.0017}$	$0.0204^{+0.0017}_{-0.0043}$	$-20.2238^{+0.0246}_{-0.0331}$	$0.7128^{+0.0017}_{-0.0017}$	$0.0199^{+0.0017}_{-0.0043}$
20080228	$-20.3550^{+0.0198}_{-0.0411}$	$0.7140^{+0.0013}_{-0.0018}$	$0.0117^{+0.0040}_{-0.0021}$	$-20.3615^{+0.0183}_{-0.0281}$	$0.7131^{+0.0011}_{-0.0018}$	$0.0111^{+0.0042}_{-0.0020}$
20090222	$-20.3963^{+0.0152}_{-0.0426}$	$0.7153^{+0.0009}_{-0.0016}$	$0.0061^{+0.0067}_{-0.0020}$	$-20.3904^{+0.0203}_{-0.0349}$	$0.7158^{+0.0010}_{-0.0018}$	$0.0084^{+0.0056}_{-0.0016}$
20100217	$-20.4220^{+0.0216}_{-0.0280}$	$0.7098^{+0.0012}_{-0.0017}$	$0.0150^{+0.0026}_{-0.0027}$	$-20.4250^{+0.0217}_{-0.0240}$	$0.7113^{+0.0012}_{-0.0018}$	$0.0151^{+0.0026}_{-0.0028}$
20110212	$-20.4380^{+0.0205}_{-0.0222}$	$0.7123^{+0.0010}_{-0.0020}$	$0.0099^{+0.0044}_{-0.0019}$	$-20.4282^{+0.0208}_{-0.0247}$	$0.7134^{+0.0011}_{-0.0020}$	$0.0097^{+0.0047}_{-0.0019}$
20120207	$-20.4451^{+0.0227}_{-0.0325}$	$0.7095^{+0.0015}_{-0.0018}$	$0.0179^{+0.0021}_{-0.0035}$	$-20.4325^{+0.0194}_{-0.0246}$	$0.7073^{+0.0014}_{-0.0014}$	$0.0189^{+0.0015}_{-0.0040}$
20130201	$-20.4804^{+0.0209}_{-0.0163}$	$0.7119^{+0.0009}_{-0.0018}$	$0.0105^{+0.0040}_{-0.0019}$	$-20.4477^{+0.0219}_{-0.0208}$	$0.7068^{+0.0011}_{-0.0018}$	$0.0113^{+0.0039}_{-0.0020}$
20140127	$-20.5172^{+0.0237}_{-0.0261}$	$0.7096^{+0.0014}_{-0.0017}$	$0.0169^{+0.0022}_{-0.0035}$	$-20.4897^{+0.0233}_{-0.0250}$	$0.7095^{+0.0013}_{-0.0017}$	$0.0154^{+0.0026}_{-0.0029}$
20150122	$-20.4477^{+0.0238}_{-0.0257}$	$0.7124^{+0.0009}_{-0.0018}$	$0.0096^{+0.0043}_{-0.0017}$	$-20.4303^{+0.0210}_{-0.0223}$	$0.7113^{+0.0010}_{-0.0018}$	$0.0109^{+0.0040}_{-0.0018}$
20160117	$-20.4954^{+0.0193}_{-0.0234}$	$0.7108^{+0.0010}_{-0.0017}$	$0.0106^{+0.0041}_{-0.0020}$	$-20.5025^{+0.0182}_{-0.0262}$	$0.7113^{+0.0012}_{-0.0018}$	$0.0121^{+0.0036}_{-0.0022}$
20170111	$-20.5844^{+0.0194}_{-0.0254}$	$0.7135^{+0.0014}_{-0.0017}$	$0.0177^{+0.0021}_{-0.0036}$	$-20.5806^{+0.0261}_{-0.0219}$	$0.7168^{+0.0014}_{-0.0017}$	$0.0167^{+0.0018}_{-0.0039}$
20180106	$-20.6863^{+0.0198}_{-0.0295}$	$0.7154^{+0.0011}_{-0.0018}$	$0.0110^{+0.0041}_{-0.0020}$	$-20.6612^{+0.0200}_{-0.0327}$	$0.7162^{+0.0012}_{-0.0019}$	$0.0101^{+0.0046}_{-0.0018}$
20190101	$-20.7515^{+0.0236}_{-0.0231}$	$0.7141^{+0.0012}_{-0.0016}$	$0.0134^{+0.0031}_{-0.0027}$	$-20.7356^{+0.0227}_{-0.0217}$	$0.7088^{+0.0013}_{-0.0018}$	$0.0164^{+0.0024}_{-0.0033}$
20191227	$-20.7444^{+0.0207}_{-0.0230}$	$0.7096^{+0.0012}_{-0.0016}$	$0.0151^{+0.0025}_{-0.0030}$	$-20.7342^{+0.0194}_{-0.0265}$	$0.7072^{+0.0013}_{-0.0016}$	$0.0156^{+0.0024}_{-0.0033}$
20201221	$-20.6563^{+0.0214}_{-0.0236}$	$0.7112^{+0.0011}_{-0.0016}$	$0.0118^{+0.0035}_{-0.0020}$	$-20.6640^{+0.0163}_{-0.0281}$	$0.7128^{+0.0012}_{-0.0017}$	$0.0134^{+0.0032}_{-0.0022}$
			MDI			
19960501	$-20.1316^{+0.0204}_{-0.0304}$	$0.715^{+0.0013}_{-0.0017}$	$0.012^{+0.0038}_{-0.0024}$	$-20.098^{+0.0171}_{-0.0371}$	$0.716^{+0.0012}_{-0.0019}$	$0.011^{+0.0045}_{-0.0018}$
19970426	$-20.0283^{+0.0170}_{-0.0358}$	$0.712^{+0.0014}_{-0.0018}$	$0.013^{+0.0034}_{-0.0027}$	$-19.982^{+0.0241}_{-0.0298}$	$0.712^{+0.0013}_{-0.0019}$	$0.012^{+0.0038}_{-0.0023}$
19980421	$-19.8181^{+0.0143}_{-0.0293}$	$0.712^{+0.0009}_{-0.0016}$	$0.003^{+0.0071}_{-0.0025}$	$-19.781^{+0.0155}_{-0.0147}$	$0.714^{+0.0007}_{-0.0017}$	$0.004^{+0.0073}_{-0.0028}$
19990416	$-19.5900^{+0.0137}_{-0.0105}$	$0.708^{+0.0006}_{-0.0013}$	$0.004^{+0.0072}_{-0.0029}$	$-19.587^{+0.0185}_{-0.0188}$	$0.715^{+0.0012}_{-0.0019}$	$0.012^{+0.0038}_{-0.0025}$
20000410	$-19.5399^{+0.0180}_{-0.0361}$	$0.714^{+0.0014}_{-0.0017}$	$0.014^{+0.0032}_{-0.0026}$	$-19.528^{+0.0191}_{-0.0356}$	$0.714^{+0.0014}_{-0.0019}$	$0.013^{+0.0036}_{-0.0026}$
20010405	$-19.4541^{+0.0207}_{-0.0323}$	$0.716^{+0.0014}_{-0.0017}$	$0.013^{+0.0033}_{-0.0024}$	$-19.398^{+0.0187}_{-0.0412}$	$0.718^{+0.0012}_{-0.0021}$	$0.011^{+0.0044}_{-0.0020}$
20020331	$-19.4452^{+0.0264}_{-0.0316}$	$0.716^{+0.0014}_{-0.0016}$	$0.015^{+0.0026}_{-0.0033}$	$-19.402^{+0.0259}_{-0.0236}$	$0.711^{+0.0012}_{-0.0021}$	$0.010^{+0.0049}_{-0.0022}$
20030326	$-19.4798^{+0.0154}_{-0.0312}$	$0.714^{+0.0014}_{-0.0017}$	$0.014^{+0.0028}_{-0.0027}$	$-19.484^{+0.0217}_{-0.0258}$	$0.716^{+0.0015}_{-0.0018}$	$0.017^{+0.0021}_{-0.0037}$
20040320	$-19.7038^{+0.0204}_{-0.0300}$	$0.713^{+0.0014}_{-0.0014}$	$0.018^{+0.0020}_{-0.0035}$	$-19.701^{+0.0213}_{-0.0372}$	$0.714^{+0.0016}_{-0.0020}$	$0.017^{+0.0023}_{-0.0035}$
20050315	$-19.8893^{+0.0241}_{-0.0401}$	$0.715^{+0.0016}_{-0.0018}$	$0.015^{+0.0027}_{-0.0031}$	$-19.869^{+0.0177}_{-0.0367}$	$0.716^{+0.0012}_{-0.0018}$	$0.012^{+0.0039}_{-0.0023}$
20060310	$-20.0228^{+0.0186}_{-0.0259}$	$0.710^{+0.0013}_{-0.0018}$	$0.011^{+0.0041}_{-0.0022}$	$-19.977^{+0.0168}_{-0.0276}$	$0.711^{+0.0013}_{-0.0020}$	$0.012^{+0.0038}_{-0.0023}$
20070305	$-20.2526^{+0.0262}_{-0.0342}$	$0.710^{+0.0017}_{-0.0017}$	$0.019^{+0.0019}_{-0.0042}$	$-20.191^{+0.0213}_{-0.0284}$	$0.711^{+0.0015}_{-0.0018}$	$0.016^{+0.0024}_{-0.0033}$
20080228	$-20.3209^{+0.0163}_{-0.0243}$	$0.711^{+0.0010}_{-0.0016}$	$0.007^{+0.0057}_{-0.0016}$	$-20.333^{+0.0220}_{-0.0268}$	$0.711^{+0.0013}_{-0.0018}$	$0.012^{+0.0037}_{-0.0023}$
20090222	$-20.4334^{+0.0206}_{-0.0425}$	$0.715^{+0.0014}_{-0.0019}$	$0.009^{+0.0051}_{-0.0020}$	$-20.410^{+0.0148}_{-0.0269}$	$0.713^{+0.0009}_{-0.0017}$	$0.009^{+0.0064}_{-0.0016}$
20100217	$-20.4412^{+0.0221}_{-0.0258}$	$0.708^{+0.0014}_{-0.0016}$	$0.014^{+0.0026}_{-0.0030}$	$-20.417^{+0.0209}_{-0.0256}$	$0.709^{+0.0012}_{-0.0019}$	$0.012^{+0.0036}_{-0.0025}$
			HMI			
20110212	$-20.3896^{+0.0129}_{-0.0118}$	$0.7101^{+0.0005}_{-0.0011}$	$0.0084^{+0.0065}_{-0.0024}$	$-20.3791^{+0.0116}_{-0.0207}$	$0.7108^{+0.0007}_{-0.0014}$	$0.0093^{+0.0066}_{-0.0026}$
20120207	$-20.4144^{+0.0225}_{-0.0192}$	$0.7101^{+0.0014}_{-0.0015}$	$0.0168^{+0.0017}_{-0.0041}$	$-20.3916^{+0.0208}_{-0.0242}$	$0.7088^{+0.0012}_{-0.0014}$	$0.0162^{+0.0023}_{-0.0031}$
20130201	$-20.4916^{+0.0207}_{-0.0221}$	$0.7115^{+0.0011}_{-0.0015}$	$0.0126^{+0.0030}_{-0.0024}$	$-20.4691^{+0.0159}_{-0.0198}$	$0.7107^{+0.0009}_{-0.0015}$	$0.0105^{+0.0036}_{-0.0018}$
20140127	$-20.4939^{+0.0250}_{-0.0260}$	$0.7096^{+0.0015}_{-0.0014}$	$0.0164^{+0.0017}_{-0.0045}$	$-20.4656^{+0.0213}_{-0.0197}$	$0.7058^{+0.0013}_{-0.0016}$	$0.0148^{+0.0025}_{-0.0033}$
20150122	$-20.4306^{+0.0178}_{-0.0189}$	$0.7104^{+0.0011}_{-0.0016}$	$0.0125^{+0.0030}_{-0.0022}$	$-20.4491^{+0.0191}_{-0.0231}$	$0.7106^{+0.0012}_{-0.0016}$	$0.0136^{+0.0029}_{-0.0025}$
20160117	$-20.5281^{+0.0158}_{-0.0275}$	$0.7131^{+0.0012}_{-0.0017}$	$0.0105^{+0.0042}_{-0.0021}$	$-20.5102^{+0.0172}_{-0.0302}$	$0.7123^{+0.0013}_{-0.0017}$	$0.0126^{+0.0034}_{-0.0025}$
20170111	$-20.6053^{+0.0196}_{-0.0347}$	$0.7111^{+0.0018}_{-0.0015}$	$0.0119^{+0.0015}_{-0.0046}$	$-20.6001^{+0.0208}_{-0.0307}$	$0.7155^{+0.0016}_{-0.0016}$	$0.0182^{+0.0017}_{-0.0042}$
20180106	$-20.6852^{+0.0200}_{-0.0354}$	$0.7166^{+0.0013}_{-0.0017}$	$0.0117^{+0.0040}_{-0.0023}$	$-20.6706^{+0.0225}_{-0.0301}$	$0.7146^{+0.0013}_{-0.0017}$	$0.0125^{+0.0036}_{-0.0025}$
20190101	$-20.7105^{+0.0189}_{-0.0190}$	$0.7128^{+0.0010}_{-0.0016}$	$0.0108^{+0.0037}_{-0.0022}$	$-20.7045^{+0.0199}_{-0.0185}$	$0.7085^{+0.0011}_{-0.0016}$	$0.0115^{+0.0034}_{-0.0023}$
20191227	$-20.7168^{+0.0219}_{-0.0198}$	$0.7102^{+0.0012}_{-0.0017}$	$0.0100^{+0.0042}_{-0.0022}$	$-20.6952^{+0.0211}_{-0.0229}$	$0.7100^{+0.0011}_{-0.0016}$	$0.0088^{+0.0049}_{-0.0019}$
20201221	$-20.6716^{+0.0190}_{-0.0212}$	$0.7102^{+0.0012}_{-0.0018}$	$0.0110^{+0.0037}_{-0.0020}$	$-20.6491^{+0.0198}_{-0.0246}$	$0.7092^{+0.0012}_{-0.0018}$	$0.0121^{+0.0034}_{-0.0025}$
20211216	$-20.5538^{+0.0168}_{-0.0161}$	$0.7141^{+0.0006}_{-0.0015}$	$0.0031^{+0.0068}_{-0.0026}$	$-20.5291^{+0.0154}_{-0.0112}$	$0.7133^{+0.0006}_{-0.0016}$	$0.0036^{+0.0067}_{-0.0027}$

Table 5. Tachocline from 5 × 72-day official pipeline sets

Start Date	$\delta\Omega/2\pi$ (nHz)	r_d ($R_\odot$)	w_d ($R_\odot$)	Start Date	$\delta\Omega/2\pi$ (nHz)	r_d ($R_\odot$)	w_d ($R_\odot$)
	Asymmetric Fits				Symmetric Fits		
			MDI				
19960501	$-19.7402^{+0.0154}_{-0.0467}$	$0.7130^{+0.0011}_{-0.0021}$	$0.0090^{+0.0056}_{-0.0017}$	19960501	$-19.7107^{+0.0142}_{-0.0565}$	$0.7190^{+0.0011}_{-0.0021}$	$0.0074^{+0.0054}_{-0.0014}$
19970426	$-19.5804^{+0.0195}_{-0.0454}$	$0.7146^{+0.0014}_{-0.0022}$	$0.0138^{+0.0034}_{-0.0024}$	19960712	$-19.7026^{+0.0210}_{-0.0464}$	$0.7197^{+0.0012}_{-0.0023}$	$0.0112^{+0.0039}_{-0.0017}$
19980421	$-19.2731^{+0.0140}_{-0.0451}$	$0.7104^{+0.0008}_{-0.0019}$	$0.0060^{+0.0080}_{-0.0032}$	19970426	$-19.5795^{+0.0152}_{-0.0427}$	$0.7144^{+0.0014}_{-0.0021}$	$0.0129^{+0.0024}_{-0.0021}$
19990416	$-19.2008^{+0.0216}_{-0.0390}$	$0.7161^{+0.0012}_{-0.0023}$	$0.0101^{+0.0051}_{-0.0019}$	19970707	$-19.5339^{+0.0214}_{-0.0426}$	$0.7163^{+0.0013}_{-0.0022}$	$0.0130^{+0.0029}_{-0.0018}$
20000410	$-19.1108^{+0.0209}_{-0.0563}$	$0.7122^{+0.0014}_{-0.0024}$	$0.0164^{+0.0029}_{-0.0031}$	19980421	$-19.2442^{+0.0154}_{-0.0359}$	$0.7197^{+0.0007}_{-0.0019}$	$0.0049^{+0.0060}_{-0.0019}$
20010405	$-18.9559^{+0.0164}_{-0.0516}$	$0.7171^{+0.0011}_{-0.0023}$	$0.0085^{+0.0061}_{-0.0017}$	19980702	$-19.2419^{+0.0227}_{-0.0562}$	$0.7164^{+0.0015}_{-0.0021}$	$0.0104^{+0.0024}_{-0.0022}$
20020331	$-19.0240^{+0.0231}_{-0.0403}$	$0.7154^{+0.0013}_{-0.0023}$	$0.0125^{+0.0039}_{-0.0023}$	19990416	$-19.1809^{+0.0182}_{-0.0424}$	$0.7155^{+0.0013}_{-0.0022}$	$0.0104^{+0.0040}_{-0.0016}$
20030326	$-19.1309^{+0.0180}_{-0.0349}$	$0.7153^{+0.0012}_{-0.0022}$	$0.0107^{+0.0045}_{-0.0019}$	19990627	$-19.1270^{+0.0172}_{-0.0414}$	$0.7162^{+0.0011}_{-0.0022}$	$0.0082^{+0.0047}_{-0.0013}$
20040320	$-19.3317^{+0.0166}_{-0.0509}$	$0.7152^{+0.0015}_{-0.0021}$	$0.0143^{+0.0035}_{-0.0025}$	20000410	$-19.0751^{+0.0192}_{-0.0549}$	$0.7188^{+0.0014}_{-0.0023}$	$0.0106^{+0.0023}_{-0.0023}$
20050315	$-19.5403^{+0.0234}_{-0.0670}$	$0.7168^{+0.0014}_{-0.0024}$	$0.0163^{+0.0031}_{-0.0028}$	20000621	$-19.0093^{+0.0158}_{-0.0563}$	$0.7209^{+0.0012}_{-0.0024}$	$0.0090^{+0.0046}_{-0.0013}$
20060310	$-19.6391^{+0.0242}_{-0.0473}$	$0.7158^{+0.0014}_{-0.0019}$	$0.0171^{+0.0024}_{-0.0031}$	20010405	$-18.9305^{+0.0180}_{-0.0600}$	$0.7215^{+0.0012}_{-0.0023}$	$0.0096^{+0.0043}_{-0.0014}$
20070305	$-19.8643^{+0.0238}_{-0.0535}$	$0.7166^{+0.0015}_{-0.0020}$	$0.0169^{+0.0026}_{-0.0032}$	20010616	$-18.9230^{+0.0185}_{-0.0480}$	$0.7207^{+0.0011}_{-0.0024}$	$0.0085^{+0.0049}_{-0.0014}$
20080228	$-20.0842^{+0.0196}_{-0.0524}$	$0.7147^{+0.0015}_{-0.0019}$	$0.0180^{+0.0023}_{-0.0033}$	20020331	$-18.9884^{+0.0196}_{-0.0444}$	$0.7147^{+0.0014}_{-0.0025}$	$0.0120^{+0.0033}_{-0.0017}$
20090222	$-20.1251^{+0.0200}_{-0.0549}$	$0.7175^{+0.0011}_{-0.0021}$	$0.0087^{+0.0057}_{-0.0018}$	20020611	$-19.0493^{+0.0165}_{-0.0517}$	$0.7148^{+0.0013}_{-0.0021}$	$0.0145^{+0.0025}_{-0.0019}$
20100217	$-20.0711^{+0.0180}_{-0.0453}$	$0.7116^{+0.0011}_{-0.0021}$	$0.0103^{+0.0046}_{-0.0018}$	20030326	$-19.1230^{+0.0199}_{-0.0372}$	$0.7156^{+0.0012}_{-0.0023}$	$0.0104^{+0.0036}_{-0.0015}$
				20030606	$-19.1684^{+0.0144}_{-0.0460}$	$0.7151^{+0.0011}_{-0.0022}$	$0.0097^{+0.0042}_{-0.0014}$
				20040320	$-19.3306^{+0.0201}_{-0.0411}$	$0.7141^{+0.0016}_{-0.0022}$	$0.0165^{+0.0021}_{-0.0026}$
				20040531	$-19.3573^{+0.0247}_{-0.0466}$	$0.7153^{+0.0016}_{-0.0022}$	$0.0171^{+0.0019}_{-0.0029}$
				20050315	$-19.5088^{+0.0190}_{-0.0569}$	$0.7204^{+0.0013}_{-0.0023}$	$0.0159^{+0.0025}_{-0.0022}$
				20050526	$-19.5710^{+0.0215}_{-0.0572}$	$0.7206^{+0.0014}_{-0.0021}$	$0.0167^{+0.0021}_{-0.0024}$
				20060310	$-19.6401^{+0.0256}_{-0.0483}$	$0.7167^{+0.0014}_{-0.0023}$	$0.0165^{+0.0021}_{-0.0024}$
				20060521	$-19.7056^{+0.0230}_{-0.0527}$	$0.7181^{+0.0015}_{-0.0022}$	$0.0163^{+0.0022}_{-0.0024}$
				20070305	$-19.8355^{+0.0227}_{-0.0492}$	$0.7170^{+0.0014}_{-0.0020}$	$0.0168^{+0.0020}_{-0.0024}$
				20070516	$-19.8760^{+0.0207}_{-0.0482}$	$0.7182^{+0.0014}_{-0.0021}$	$0.0143^{+0.0028}_{-0.0020}$
				20080228	$-20.0280^{+0.0231}_{-0.0500}$	$0.7176^{+0.0015}_{-0.0020}$	$0.0167^{+0.0021}_{-0.0024}$
				20080510	$-20.0698^{+0.0243}_{-0.0494}$	$0.7207^{+0.0013}_{-0.0021}$	$0.0140^{+0.0029}_{-0.0019}$
				20090222	$-20.1139^{+0.0174}_{-0.0560}$	$0.7209^{+0.0011}_{-0.0021}$	$0.0093^{+0.0044}_{-0.0013}$
				20090505	$-20.1131^{+0.0225}_{-0.0460}$	$0.7183^{+0.0013}_{-0.0020}$	$0.0128^{+0.0031}_{-0.0018}$
				20100217	$-20.0563^{+0.0185}_{-0.0442}$	$0.7169^{+0.0012}_{-0.0019}$	$0.0103^{+0.0037}_{-0.0014}$
				20100430	$-20.0766^{+0.0206}_{-0.0470}$	$0.7182^{+0.0012}_{-0.0020}$	$0.0130^{+0.0028}_{-0.0017}$
			HMI				
20100430	$-20.3000^{+0.0168}_{-0.0374}$	$0.7142^{+0.0010}_{-0.0018}$	$0.0116^{+0.0030}_{-0.0015}$	20100430	$-20.2894^{+0.0182}_{-0.0370}$	$0.7143^{+0.0011}_{-0.0019}$	$0.0121^{+0.0027}_{-0.0016}$
20100711	$-20.3075^{+0.0219}_{-0.0324}$	$0.7137^{+0.0011}_{-0.0020}$	$0.0116^{+0.0028}_{-0.0015}$	20100711	$-20.2956^{+0.0178}_{-0.0321}$	$0.7137^{+0.0011}_{-0.0019}$	$0.0112^{+0.0030}_{-0.0013}$
20110212	$-20.2708^{+0.0160}_{-0.0355}$	$0.7147^{+0.0009}_{-0.0018}$	$0.0092^{+0.0035}_{-0.0011}$	20110212	$-20.2668^{+0.0160}_{-0.0408}$	$0.7149^{+0.0011}_{-0.0020}$	$0.0095^{+0.0037}_{-0.0013}$
20110425	$-20.2503^{+0.0195}_{-0.0294}$	$0.7133^{+0.0010}_{-0.0019}$	$0.0108^{+0.0030}_{-0.0014}$	20110425	$-20.2412^{+0.0199}_{-0.0349}$	$0.7142^{+0.0010}_{-0.0018}$	$0.0097^{+0.0035}_{-0.0013}$
20110706	$-20.2145^{+0.0190}_{-0.0318}$	$0.7137^{+0.0010}_{-0.0017}$	$0.0104^{+0.0032}_{-0.0013}$	20110706	$-20.2006^{+0.0186}_{-0.0307}$	$0.7139^{+0.0010}_{-0.0018}$	$0.0103^{+0.0032}_{-0.0013}$
20120207	$-20.2657^{+0.0200}_{-0.0378}$	$0.7103^{+0.0013}_{-0.0017}$	$0.0168^{+0.0015}_{-0.0025}$	20120207	$-20.2598^{+0.0201}_{-0.0313}$	$0.7105^{+0.0013}_{-0.0018}$	$0.0171^{+0.0016}_{-0.0025}$
20120419	$-20.2677^{+0.0189}_{-0.0375}$	$0.7124^{+0.0011}_{-0.0018}$	$0.0136^{+0.0023}_{-0.0017}$	20120419	$-20.2688^{+0.0201}_{-0.0323}$	$0.7117^{+0.0012}_{-0.0018}$	$0.0144^{+0.0021}_{-0.0019}$
20120630	$-20.2885^{+0.0185}_{-0.0261}$	$0.7119^{+0.0010}_{-0.0018}$	$0.0110^{+0.0029}_{-0.0013}$	20120630	$-20.2828^{+0.0169}_{-0.0305}$	$0.7116^{+0.0010}_{-0.0018}$	$0.0110^{+0.0029}_{-0.0014}$
20130201	$-20.3178^{+0.0185}_{-0.0266}$	$0.7127^{+0.0009}_{-0.0018}$	$0.0096^{+0.0033}_{-0.0012}$	20130201	$-20.3050^{+0.0217}_{-0.0262}$	$0.7127^{+0.0010}_{-0.0020}$	$0.0089^{+0.0036}_{-0.0012}$
20130414	$-20.3502^{+0.0192}_{-0.0355}$	$0.7138^{+0.0011}_{-0.0019}$	$0.0114^{+0.0030}_{-0.0015}$	20130414	$-20.3286^{+0.0173}_{-0.0313}$	$0.7133^{+0.0010}_{-0.0019}$	$0.0115^{+0.0028}_{-0.0015}$
20130625	$-20.3484^{+0.0159}_{-0.0329}$	$0.7143^{+0.0010}_{-0.0018}$	$0.0116^{+0.0028}_{-0.0014}$	20130625	$-20.3457^{+0.0149}_{-0.0333}$	$0.7145^{+0.0011}_{-0.0018}$	$0.0115^{+0.0028}_{-0.0015}$
20140127	$-20.3432^{+0.0217}_{-0.0417}$	$0.7122^{+0.0013}_{-0.0017}$	$0.0160^{+0.0019}_{-0.0022}$	20140127	$-20.3306^{+0.0198}_{-0.0365}$	$0.7120^{+0.0014}_{-0.0018}$	$0.0160^{+0.0019}_{-0.0023}$
20140409	$-20.3606^{+0.0179}_{-0.0343}$	$0.7131^{+0.0014}_{-0.0017}$	$0.0162^{+0.0018}_{-0.0022}$	20140409	$-20.3514^{+0.0206}_{-0.0370}$	$0.7130^{+0.0014}_{-0.0019}$	$0.0162^{+0.0019}_{-0.0023}$
20140620	$-20.3671^{+0.0180}_{-0.0478}$	$0.7142^{+0.0013}_{-0.0019}$	$0.0149^{+0.0023}_{-0.0019}$	20140620	$-20.3601^{+0.0189}_{-0.0415}$	$0.7139^{+0.0013}_{-0.0018}$	$0.0157^{+0.0019}_{-0.0019}$
20150122	$-20.3464^{+0.0160}_{-0.0338}$	$0.7142^{+0.0011}_{-0.0018}$	$0.0135^{+0.0023}_{-0.0016}$	20150122	$-20.3398^{+0.0190}_{-0.0380}$	$0.7138^{+0.0011}_{-0.0016}$	$0.0132^{+0.0023}_{-0.0015}$
20150404	$-20.3526^{+0.0218}_{-0.0344}$	$0.7131^{+0.0012}_{-0.0018}$	$0.0134^{+0.0024}_{-0.0018}$	20150404	$-20.3478^{+0.0189}_{-0.0361}$	$0.7134^{+0.0012}_{-0.0020}$	$0.0137^{+0.0024}_{-0.0017}$
20150615	$-20.3832^{+0.0219}_{-0.0389}$	$0.7111^{+0.0012}_{-0.0018}$	$0.0146^{+0.0022}_{-0.0020}$	20150615	$-20.3688^{+0.0184}_{-0.0277}$	$0.7105^{+0.0011}_{-0.0016}$	$0.0139^{+0.0021}_{-0.0019}$
20160117	$-20.3555^{+0.0168}_{-0.0386}$	$0.7134^{+0.0011}_{-0.0019}$	$0.0119^{+0.0029}_{-0.0015}$	20160117	$-20.3464^{+0.0194}_{-0.0300}$	$0.7133^{+0.0011}_{-0.0018}$	$0.0125^{+0.0025}_{-0.0016}$
20160329	$-20.3969^{+0.0171}_{-0.0362}$	$0.7137^{+0.0013}_{-0.0017}$	$0.0142^{+0.0022}_{-0.0019}$	20160329	$-20.3948^{+0.0153}_{-0.0448}$	$0.7137^{+0.0013}_{-0.0018}$	$0.0142^{+0.0024}_{-0.0018}$
20160609	$-20.3899^{+0.0188}_{-0.0358}$	$0.7144^{+0.0012}_{-0.0018}$	$0.0139^{+0.0022}_{-0.0018}$	20160609	$-20.3788^{+0.0217}_{-0.0388}$	$0.7145^{+0.0012}_{-0.0019}$	$0.0128^{+0.0025}_{-0.0016}$
20170111	$-20.4268^{+0.0217}_{-0.0409}$	$0.7141^{+0.0015}_{-0.0018}$	$0.0172^{+0.0017}_{-0.0024}$	20170111	$-20.4398^{+0.0186}_{-0.0424}$	$0.7139^{+0.0013}_{-0.0018}$	$0.0175^{+0.0016}_{-0.0022}$
20170324	$-20.4372^{+0.0197}_{-0.0371}$	$0.7154^{+0.0011}_{-0.0017}$	$0.0137^{+0.0021}_{-0.0016}$	20170324	$-20.4448^{+0.0200}_{-0.0378}$	$0.7156^{+0.0010}_{-0.0017}$	$0.0139^{+0.0022}_{-0.0017}$
20170604	$-20.4723^{+0.0178}_{-0.0345}$	$0.7158^{+0.0011}_{-0.0019}$	$0.0113^{+0.0030}_{-0.0014}$	20170604	$-20.4680^{+0.0190}_{-0.0374}$	$0.7163^{+0.0011}_{-0.0018}$	$0.0118^{+0.0030}_{-0.0014}$
20180319	$-20.5866^{+0.0172}_{-0.0441}$	$0.7159^{+0.0012}_{-0.0019}$	$0.0127^{+0.0027}_{-0.0016}$	20180106	$-20.5350^{+0.0189}_{-0.0283}$	$0.7151^{+0.0010}_{-0.0018}$	$0.0101^{+0.0033}_{-0.0014}$
20180530	$-20.5797^{+0.0134}_{-0.0368}$	$0.7153^{+0.0010}_{-0.0018}$	$0.0089^{+0.0036}_{-0.0012}$	20180319	$-20.5561^{+0.0190}_{-0.0388}$	$0.7155^{+0.0012}_{-0.0019}$	$0.0118^{+0.0028}_{-0.0016}$
20190314	$-20.6050^{+0.0179}_{-0.0258}$	$0.7116^{+0.0010}_{-0.0019}$	$0.0092^{+0.0033}_{-0.0012}$	20180530	$-20.5605^{+0.0167}_{-0.0337}$	$0.7150^{+0.0010}_{-0.0019}$	$0.0090^{+0.0037}_{-0.0013}$
20191016	$-20.5351^{+0.0174}_{-0.0344}$	$0.7099^{+0.0012}_{-0.0017}$	$0.0147^{+0.0013}_{-0.0025}$	20190314	$-20.5972^{+0.0186}_{-0.0309}$	$0.7117^{+0.0009}_{-0.0018}$	$0.0095^{+0.0031}_{-0.0012}$
20210303	$-20.5367^{+0.0193}_{-0.0291}$	$0.7119^{+0.0011}_{-0.0016}$	$0.0150^{+0.0017}_{-0.0020}$	20191016	$-20.5418^{+0.0113}_{-0.0376}$	$0.7101^{+0.0015}_{-0.0018}$	$0.0194^{+0.0012}_{-0.0028}$
				20210303	$-20.5282^{+0.0193}_{-0.0330}$	$0.7120^{+0.0011}_{-0.0017}$	$0.0145^{+0.0019}_{-0.0019}$
				20220226	$-20.3904^{+0.0199}_{-0.0288}$	$0.7124^{+0.0010}_{-0.0017}$	$0.0133^{+0.0020}_{-0.0016}$

Table 6. Tachocline properties from 8 × 72-day SGK sets

Start Date	$\delta\Omega/2\pi$ (nHz)	r_d ($R_\odot$)	w_d ($R_\odot$)	$\delta\Omega/2\pi$ (nHz)	r_d ($R_\odot$)	w_d ($R_\odot$)
		GONG			MDI	
19950718	-19.9715 ± 0.0117	0.7090 ± 0.0012	0.0098 ± 0.0017			
19960501	-20.0201 ± 0.0182	0.7131 ± 0.0011	0.0114 ± 0.0016	-20.0907 ± 0.0194	0.7144 ± 0.0011	0.0128 ± 0.0016
19970213	-19.9300 ± 010248	0.7098 ± 0.0011	0.0148 ± 0.0015	-19.9548 ± 0.0138	0.7083 ± 0.0012	0.0149 ± 0.0016
19971128	-19.8463 ± 0.0154	0.7119 ± 0.0012	0.0106 ± 0.0016	-19.8492 ± 0.0196	0.7098 ± 0.0011	0.0063 ± 0.0016
19980912	-19.7477 ± 0.0113	0.7101 ± 0.0011	0.0090 ± 0.0013	-19.6535 ± 0.0163	0.7089 ± 0.0011	0.0108 ± 0.0016
19990627	-19.5548 ± 0.0135	0.7067 ± 0.0015	0.0101 ± 0.0016	-19.5295 ± 0.0133	0.7082 ± 0.0015	0.0090 ± 0.0016
20000410	-19.4879 ± 0.0157	0.7163 ± 0.0017	0.0102 ± 0.0016	-19.4582 ± 0.0172	0.7181 ± 0.0011	0.0104 ± 0.0016
20010123	-19.4365 ± 0.0104	0.7187 ± 0.0012	0.0107 ± 0.0015	-19.4034 ± 0.0163	0.7176 ± 0.0011	0.0105 ± 0.0016
20011107	-19.3821 ± 0.0119	0.7102 ± 0.0011	0.0148 ± 0.0016	-19.4349 ± 0.0178	0.7092 ± 0.0018	0.0175 ± 0.0016
20020822	-19.4426 ± 0.0119	0.7068 ± 0.0013	0.0126 ± 0.0016	-19.4919 ± 0.0138	0.7083 ± 0.0011	0.0148 ± 0.0016
20030606	-19.6120 ± 0.0184	0.7132 ± 0.0017	0.0171 ± 0.0018	-19.6135 ± 0.0169	0.7121 ± 0.0010	0.0147 ± 0.0016
20040320	-19.6995 ± 0.0104	0.7129 ± 0.0014	0.0192 ± 0.0016	-19.7519 ± 0.0162	0.7137 ± 0.0011	0.0175 ± 0.0016
20050102	-19.8570 ± 0.0171	0.7132 ± 0.0013	0.0198 ± 0.0016	-19.8490 ± 0.0148	0.7156 ± 0.0012	0.0143 ± 0.0016
20051017	-19.9651 ± 0.0194	0.7134 ± 0.0012	0.0103 ± 0.0019	-19.9920 ± 0.0196	0.7139 ± 0.0011	0.0136 ± 0.0016
20060801	-20.1474 ± 0.0124	0.7130 ± 0.0011	0.0173 ± 0.0012	-20.1492 ± 0.0119	0.7142 ± 0.0011	0.0186 ± 0.0016
20070516	-20.3080 ± 0.0135	0.7113 ± 0.0013	0.0164 ± 0.0016	-20.2940 ± 0.0174	0.7115 ± 0.0015	0.0142 ± 0.0016
20080228	-20.3843 ± 0.0100	0.7146 ± 0.0014	0.0116 ± 0.0013	-20.3927 ± 0.0106	0.7116 ± 0.0012	0.0094 ± 0.0016
20081212	-20.4449 ± 0.0111	0.7155 ± 0.0013	0.0116 ± 0.0016	-20.4403 ± 0.0140	0.7124 ± 0.0011	0.0117 ± 0.0016
20090926	-20.4509 ± 0.0189	0.7132 ± 0.0015	0.0115 ± 0.0015	-20.4508 ± 0.0125	0.7119 ± 0.0014	0.0117 ± 0.0016
					HMI	
20100711	-20.4288 ± 0.0116	0.7129 ± 0.0012	0.0133 ± 0.0016	-20.3927 ± 0.0112	0.7115 ± 0.0011	0.0126 ± 0.0016
20110425	-20.4264 ± 0.0114	0.7108 ± 0.0012	0.0144 ± 0.0017	-20.3940 ± 0.0173	0.7121 ± 0.0010	0.0133 ± 0.0014
20120207	-20.4162 ± 0.0180	0.7082 ± 0.0012	0.0152 ± 0.0013	-20.4049 ± 0.0142	0.7107 ± 0.0010	0.0135 ± 0.0014
20121121	-20.4742 ± 0.0193	0.7087 ± 0.0013	0.0125 ± 0.0016	-20.4636 ± 0.0180	0.7120 ± 0.0011	0.0090 ± 0.0015
20130905	-20.4941 ± 0.0199	0.7119 ± 0.0015	0.0155 ± 0.0012	-20.4785 ± 0.0183	0.7118 ± 0.0012	0.0125 ± 0.0014
20140620	-20.4502 ± 0.0163	0.7127 ± 0.0015	0.0119 ± 0.0011	-20.4389 ± 0.0182	0.7132 ± 0.0010	0.0107 ± 0.0016
20150404	-20.4877 ± 0.0164	0.7119 ± 0.0016	0.0105 ± 0.0010	-20.4851 ± 0.0146	0.7147 ± 0.0012	0.0097 ± 0.0017
20160117	-20.5200 ± 0.0116	0.7147 ± 0.0016	0.0129 ± 0.0011	-20.4575 ± 0.0186	0.7125 ± 0.0011	0.0117 ± 0.0015
20161031	-20.5954 ± 0.0101	0.7140 ± 0.0014	0.0150 ± 0.0014	-20.5651 ± 0.0105	0.7146 ± 0.0011	0.0137 ± 0.0016
20170815	-20.6483 ± 0.0173	0.7147 ± 0.0014	0.0108 ± 0.0017	-20.6662 ± 0.0190	0.7159 ± 0.0013	0.0124 ± 0.0017
20180530	-20.7137 ± 0.0183	0.7116 ± 0.0012	0.0122 ± 0.0019	-20.7214 ± 0.0105	0.7101 ± 0.0010	0.0113 ± 0.0014
20190314	-20.6651 ± 0.0145	0.7091 ± 0.0012	0.0077 ± 0.0015	-20.6811 ± 0.0177	0.7100 ± 0.0012	0.0094 ± 0.0011
20191227	-20.6592 ± 0.0131	0.7097 ± 0.0013	0.0109 ± 0.0015	-20.6708 ± 0.0126	0.7102 ± 0.0010	0.0129 ± 0.0015
20201010	-20.6139 ± 0.0159	0.7123 ± 0.0011	0.0105 ± 0.0017	-20.6276 ± 0.0196	0.7116 ± 0.0012	0.0109 ± 0.0014

Table 7. Tachocline properties from 10×72-day SGK sets

Start Date	$\delta\Omega/2\pi$ (nHz)	r_d ($R_\odot$)	w_d ($R_\odot$)	$\delta\Omega/2\pi$ (nHz)	r_d ($R_\odot$)	w_d ($R_\odot$)
	GONG			MDI		
19950507	-19.9427 ± 0.0118	0.7113 ± 0.0010	0.0094 ± 0.0012			
19960501	-20.0048 ± 0.0154	0.7122 ± 0.0012	0.0122 ± 0.0014	-20.0204 ± 0.0150	0.7105 ± 0.0009	0.0147 ± 0.0014
19970426	-19.8701 ± 0.0214	0.7116 ± 0.0010	0.0093 ± 0.0013	-19.9117 ± 0.0194	0.7097 ± 0.0012	0.0080 ± 0.0014
19980421	-19.7365 ± 0.0147	0.7115 ± 0.0010	0.0067 ± 0.0012	-19.6516 ± 0.0121	0.7108 ± 0.0010	0.0066 ± 0.0013
19990416	-19.5627 ± 0.0185	0.7092 ± 0.0010	0.0077 ± 0.0011	-19.5359 ± 0.0179	0.7090 ± 0.0013	0.0074 ± 0.0013
20000410	-19.4731 ± 0.0125	0.7156 ± 0.0011	0.0073 ± 0.0014	-19.4205 ± 0.0150	0.7150 ± 0.0011	0.0105 ± 0.0013
20010405	-19.3887 ± 0.0172	0.7117 ± 0.0011	0.0075 ± 0.0012	-19.4133 ± 0.0197	0.7134 ± 0.0010	0.0102 ± 0.0011
20020331	-19.4326 ± 0.0165	0.7080 ± 0.0010	0.0130 ± 0.0011	-19.4407 ± 0.0173	0.7085 ± 0.0011	0.0116 ± 0.0012
20030326	-19.5670 ± 0.0154	0.7121 ± 0.0012	0.0152 ± 0.0014	-19.5890 ± 0.0191	0.7123 ± 0.0012	0.0155 ± 0.0012
20040320	-19.7451 ± 0.0101	0.7106 ± 0.0010	0.0190 ± 0.0014	-19.7766 ± 0.0197	0.7128 ± 0.0010	0.0188 ± 0.0011
20050315	-19.9218 ± 0.0157	0.7138 ± 0.0010	0.0167 ± 0.0013	-19.9240 ± 0.0169	0.7154 ± 0.0011	0.0145 ± 0.0012
20060310	-20.0870 ± 0.0175	0.7114 ± 0.0010	0.0162 ± 0.0013	-20.1051 ± 0.0186	0.7117 ± 0.0013	0.0180 ± 0.0013
20070305	-20.3122 ± 0.0183	0.7114 ± 0.0010	0.0162 ± 0.0013	-20.3020 ± 0.0193	0.7129 ± 0.0012	0.0146 ± 0.0013
20080228	-20.4024 ± 0.0107	0.7139 ± 0.0012	0.0117 ± 0.0014	-20.3670 ± 0.0180	0.7115 ± 0.0012	0.0124 ± 0.0014
20090222	-20.4502 ± 0.0110	0.7140 ± 0.0013	0.0117 ± 0.0014	-20.4396 ± 0.0187	0.7123 ± 0.0013	0.0108 ± 0.0014
20100217	-20.4456 ± 0.0189	0.7130 ± 0.0010	0.0123 ± 0.0012		HMI	
20110212	-20.4107 ± 0.0128	0.7110 ± 0.0010	0.0145 ± 0.0012	-20.3905 ± 0.0126	0.7110 ± 0.0012	0.0137 ± 0.0014
20120207	-20.4449 ± 0.0185	0.7074 ± 0.0010	0.0146 ± 0.0013	-20.4184 ± 0.0164	0.7086 ± 0.0011	0.0134 ± 0.0013
20130201	-20.4845 ± 0.0120	0.7096 ± 0.0011	0.0129 ± 0.0013	-20.4610 ± 0.0147	0.7100 ± 0.0011	0.0115 ± 0.0013
20140127	-20.4571 ± 0.0188	0.7103 ± 0.0011	0.0127 ± 0.0013	-20.4738 ± 0.0174	0.7105 ± 0.0012	0.0138 ± 0.0012
20150122	-20.4848 ± 0.0104	0.7142 ± 0.0011	0.0110 ± 0.0014	-20.4662 ± 0.0184	0.7125 ± 0.0012	0.0108 ± 0.0012
20160117	-20.5227 ± 0.0168	0.7140 ± 0.0012	0.0145 ± 0.0014	-20.5188 ± 0.0202	0.7147 ± 0.0011	0.0132 ± 0.0011
20170111	-20.6034 ± 0.0173	0.7111 ± 0.0010	0.0153 ± 0.0012	-20.6338 ± 0.0191	0.7122 ± 0.0012	0.0157 ± 0.0012
20180106	-20.6948 ± 0.0115	0.7126 ± 0.0012	0.0133 ± 0.0014	-20.6972 ± 0.0110	0.7112 ± 0.0011	0.0138 ± 0.0011
20190101	-20.6705 ± 0.0192	0.7100 ± 0.0012	0.0112 ± 0.0014	-20.6808 ± 0.0198	0.7111 ± 0.0010	0.0097 ± 0.0011
20191227	-20.6607 ± 0.0119	0.7082 ± 0.0012	0.0143 ± 0.0014	-20.6531 ± 0.0120	0.7071 ± 0.0012	0.0140 ± 0.0012
20201221				-20.5720 ± 0.0194	0.7107 ± 0.0012	0.0083 ± 0.0013

Table 8. Tachocline properties from 16×72-day SGK sets

Start Date	$\delta\Omega/2\pi$ (nHz)	r_d ($R_\odot$)	w_d ($R_\odot$)	$\delta\Omega/2\pi$ (nHz)	r_d ($R_\odot$)	w_d ($R_\odot$)
	GONG			MDI		
19960501	-19.9262 ± 0.0107	0.7137 ± 0.0008	0.0076 ± 0.0011	-19.9428 ± 0.0110	0.7127 ± 0.0008	0.0092 ± 0.0011
19971128	-19.7035 ± 0.0115	0.7110 ± 0.0009	0.0086 ± 0.0010	-19.6422 ± 0.0118	0.7109 ± 0.0009	0.0094 ± 0.0012
19990627	-19.4843 ± 0.0171	0.7139 ± 0.0010	0.0078 ± 0.0010	-19.4708 ± 0.0118	0.7143 ± 0.0010	0.0116 ± 0.0011
20010123	-19.4542 ± 0.0153	0.7123 ± 0.0008	0.0143 ± 0.0010	-19.4566 ± 0.0125	0.7123 ± 0.0009	0.0142 ± 0.0013
20020822	-19.5802 ± 0.0126	0.7103 ± 0.0008	0.0166 ± 0.0011	-19.6231 ± 0.0112	0.7111 ± 0.0008	0.0158 ± 0.0013
20040320	-19.8293 ± 0.0147	0.7116 ± 0.0009	0.0176 ± 0.0012	-19.8706 ± 0.0119	0.7130 ± 0.0011	0.0185 ± 0.0011
20051017	-20.1392 ± 0.0127	0.7142 ± 0.0010	0.0143 ± 0.0011	-20.1435 ± 0.0106	0.7134 ± 0.0009	0.0153 ± 0.0012
20070516	-20.3578 ± 0.0118	0.7126 ± 0.0008	0.0128 ± 0.0009	-20.3540 ± 0.0114	0.7117 ± 0.0009	0.0109 ± 0.0012
20081212	-20.4374 ± 0.0100	0.7146 ± 0.0008	0.0115 ± 0.0011		HMI	
20100711	-20.4270 ± 0.0104	0.7111 ± 0.0008	0.0143 ± 0.0010	-20.3993 ± 0.0111	0.7103 ± 0.0008	0.0135 ± 0.0010
20120207	-20.4603 ± 0.0134	0.7099 ± 0.0009	0.0158 ± 0.0011	-20.4564 ± 0.0120	0.7113 ± 0.0009	0.0146 ± 0.0010
20130905	-20.4780 ± 0.0120	0.7101 ± 0.0009	0.0134 ± 0.0011	-20.4618 ± 0.0136	0.7114 ± 0.0010	0.0118 ± 0.0011
20150404	-20.5253 ± 0.0132	0.7137 ± 0.0009	0.0146 ± 0.0012	-20.4947 ± 0.0104	0.7135 ± 0.0008	0.0127 ± 0.0009
20161031	-20.6640 ± 0.0136	0.7124 ± 0.0009	0.0164 ± 0.0011	-20.6463 ± 0.0126	0.7112 ± 0.0009	0.0157 ± 0.0010
20180530	-20.6623 ± 0.0116	0.7097 ± 0.0008	0.0119 ± 0.0010	-20.6622 ± 0.0144	0.7110 ± 0.0008	0.0103 ± 0.0011

Table 9. Tachocline properties from 32×72-day SGK sets

Start Date	$\delta\Omega/2\pi$ (nHz)	r_d ($R_\odot$)	w_d ($R_\odot$)	$\delta\Omega/2\pi$ (nHz)	r_d ($R_\odot$)	w_d ($R_\odot$)
		GONG			MDI	
19960501	-19.7033 ± 0.0157	0.7134 ± 0.0005	0.0081 ± 0.0007	-19.6745 ± 0.0104	0.7132 ± 0.0006	0.0106 ± 0.0008
19990627	-19.5416 ± 0.0163	0.7121 ± 0.0006	0.0129 ± 0.0007	-19.5264 ± 0.0117	0.7129 ± 0.0005	0.0138 ± 0.0007
20020822	-19.8706 ± 0.0156	0.7119 ± 0.0006	0.0161 ± 0.0008	-19.8758 ± 0.0124	0.7124 ± 0.0007	0.0166 ± 0.0008
20051017	-20.2758 ± 0.0131	0.7143 ± 0.0004	0.0131 ± 0.0006			
20081212	-20.4341 ± 0.0132	0.7120 ± 0.0006	0.0140 ± 0.0009		HMI	
20100711	-20.4431 ± 0.0116	0.7109 ± 0.0003	0.0124 ± 0.0008	-20.4326 ± 0.0144	0.711 ± 0.0006	0.0120 ± 0.0008
20120207	-20.4788 ± 0.0159	0.7127 ± 0.0006	0.0131 ± 0.0007	-20.4788 ± 0.0108	0.712 ± 0.0004	0.0135 ± 0.0007
20150404	-20.5943 ± 0.0116	0.7118 ± 0.0005	0.0121 ± 0.0008	-20.5774 ± 0.0127	0.711 ± 0.0005	0.0122 ± 0.0008